

1 **Pharmacological modulation of AMPA receptor surface diffusion restores hippocampal**  
2 **synaptic plasticity and memory in Huntington's disease**

3

4 Hongyu Zhang<sup>1, 2</sup>, Chunlei Zhang<sup>1, 2</sup>, Jean Vincent<sup>1, 2</sup>, Diana Zala<sup>3, 4</sup>, Caroline Benstaali<sup>5, 6</sup>,  
5 Matthieu Sainlos<sup>1, 2</sup>, Dolores Grillo-Bosch<sup>1, 2</sup>, Yoon Cho<sup>7</sup>, Denis J. David<sup>8</sup>, Frederic Saudou<sup>5, 6</sup>,  
6 <sup>9</sup>, Yann Humeau<sup>1, 2</sup>, Daniel Choquet<sup>1, 2, 10-12</sup>

7

8 <sup>1</sup>Interdisciplinary Institute for Neuroscience, University of Bordeaux, Bordeaux, France.

9 <sup>2</sup>Interdisciplinary Institute for Neuroscience, Centre National de la Recherche Scientifique  
10 (CNRS) UMR 5297, Bordeaux, France.

11 <sup>3</sup>Institut Curie, CNRS, UMR3306, Inserm, U1005, F-91405 Orsay, France.

12 <sup>4</sup>ESPCI-ParisTech, PSL Research University, Paris, F-75005, France. CNRS, UMR8249,  
13 Paris, F-75005, France.

14 <sup>5</sup>Univ. Grenoble Alpes, Grenoble Institut des Neurosciences, GIN, F-38000 Grenoble, France.

15 <sup>6</sup>INSERM, U1216, F-38000, Grenoble, France.

16 <sup>7</sup> Institut de Neurosciences Cognitives et Intégratives d'Aquitaine, University of Bordeaux,  
17 France

18 <sup>8</sup> Université Paris-Saclay, Univ. Paris-Sud, Faculté de Pharmacie, CESP, INSERM  
19 UMRS1178, Chatenay-Malabry 92296, France.

20 <sup>9</sup>CHU Grenoble Alpes, F-38000, Grenoble, France.

21 <sup>10</sup>Bordeaux Imaging Center, University of Bordeaux, Bordeaux, France.

22 <sup>11</sup>Bordeaux Imaging Center, CNRS UMS 3420, Bordeaux, France.

23 <sup>12</sup>Bordeaux Imaging Center, INSERM US04, Bordeaux, France.

24 Correspondence should be addressed to D.C. ([daniel.choquet@u-bordeaux.fr](mailto:daniel.choquet@u-bordeaux.fr)), Y.H.  
25 ([yann.humeau@u-bordeaux.fr](mailto:yann.humeau@u-bordeaux.fr)) or H.Z. ([hyzhang99@hotmail.com](mailto:hyzhang99@hotmail.com)).

26

27

28

29

30 **Abstract**

31

32 Impaired hippocampal synaptic plasticity is increasingly considered to play an important role  
33 in cognitive impairment in Huntington's disease (HD). However, the molecular basis of  
34 synaptic plasticity defects is not fully understood. Combining live-cell nanoparticle tracking  
35 and super-resolution imaging, we show that dysregulation of AMPA receptors (AMPA  
36 surface diffusion represents a molecular basis underlying the aberrant hippocampal synaptic  
37 plasticity during HD. AMPARs surface diffusion is increased in various HD neuronal models,  
38 which results in the failure of AMPARs surface stabilization after long-term potentiation  
39 (LTP) stimuli. This appears to result from a defective brain-derived neurotrophic factor  
40 (BDNF) - tyrosine receptor kinase B (TrkB) - Ca<sup>2+</sup>/calmodulin-dependent protein kinase II  
41 (CaMKII) signaling pathway that impacts the interaction between the AMPAR auxiliary  
42 subunit stargazin and postsynaptic density protein 95 (PSD-95). Notably, the disturbed  
43 AMPAR surface diffusion is rescued, via BDNF signaling pathway and by the antidepressant  
44 tianeptine. Tianeptine also restores the impaired LTP and hippocampus-dependent memory as  
45 well as anxiety/depression-like behavior in different HD mouse models. We thus unveil a  
46 mechanistic framework underlying hippocampal synaptic and memory dysfunction and  
47 propose a new perspective in HD treatment by targeting AMPAR surface diffusion.

48

49

50

51

52

53

54

55

56

57

58 Cognitive deficits and psychiatric disturbance prior to motor dysfunction have been widely  
59 documented in preclinical Huntington's disease (HD) gene carriers <sup>1,2</sup>. These manifestations  
60 have traditionally been attributed to degeneration or death of corticostriatal neurons <sup>3</sup>.  
61 However, mounting evidence points to the involvement of deficits in hippocampal synaptic  
62 plasticity. This is supported by the findings that hippocampal long-term potentiation (LTP), a  
63 major form of synaptic plasticity widely regarded as a molecular basis for learning and  
64 memory, is greatly impaired in different categories of HD mouse models at pre- or early-  
65 symptomatic stage <sup>4-7</sup>. Moreover, the abnormally regained ability to support long-term  
66 depression (LTD) has also been reported in HD mice <sup>8</sup>. Consistently, behavioral studies reveal  
67 deterioration of hippocampal-associated spatial memory in distinct HD murine models <sup>7,9,10</sup>,  
68 primate model <sup>11</sup>, and patients <sup>12</sup>.

69  
70 The molecular mechanisms underlying hippocampal synaptic and memory dysfunctions are  
71 not well understood but the BDNF signaling pathway seems to play an important role. BDNF  
72 is a potent, positive modulator of LTP <sup>13</sup>. The down-regulation of its protein production <sup>6,14</sup>  
73 and the imbalance between the expression of its high-affinity TrkB receptor <sup>15,16</sup> and low-  
74 affinity p75 neurotrophin receptor (P75<sup>NTR</sup>) <sup>9,17-19</sup> have been implicated in the hippocampal  
75 synaptic and memory defects in HD. Indeed, administration of BDNF or P75<sup>NTR</sup> gene  
76 knockdown ameliorates HD-associated synaptic and memory dysfunction <sup>6,9</sup>. However, the  
77 signaling mechanisms mediating BDNF modulation of synaptic plasticity and mechanism-  
78 based pharmacological treatment strategies remain largely unexplored. This may have  
79 significant therapeutic implications as the application of exogenous BDNF is not clinically  
80 practical due to its instability in the bloodstream and its inability to cross the blood-brain  
81 barrier <sup>20,21</sup>, and genetic intervention on human subjects may carry ethical issues.

82  
83 AMPA receptors (AMPA) are the major excitatory neurotransmitter receptors. The  
84 regulated trafficking of AMPARs to and from the synapses is thought to be a key mechanism  
85 underlying glutamatergic synaptic plasticity <sup>22-24</sup>. Animal studies reveal that AMPAR

86 trafficking plays a pivotal role in experience-driven synaptic plasticity and modification of  
87 behavior <sup>25</sup>. In pathological conditions, acute stress or response to stress hormones (eg,  
88 noradrenaline, corticosterone) alters AMPAR trafficking and memory encoding processes <sup>26-</sup>  
89 <sup>28</sup>. Thus, monitoring and manipulating synaptic AMPAR trafficking emerges as a useful tool  
90 to study cognitive function and dysfunction in animal models. Synaptic delivery of AMPAR  
91 involves intracellular trafficking, insertion to the plasma membrane by exocytosis, and lateral  
92 diffusion at the neuronal surface <sup>23,29</sup>. For many years, endo/exocytosis have been considered  
93 to be the main routes for exit and entry of receptors from and to postsynaptic sites,  
94 respectively. However, our lab and others have established in the last decade that receptor  
95 surface diffusion is a key step for modifying receptor numbers at synapses <sup>22,30,31</sup>. We have  
96 demonstrated that deregulated AMPAR surface diffusion primarily contributes to the  
97 impaired LTP in stress/depression models<sup>28</sup>. Most importantly, we found that AMPAR  
98 surface diffusion can be pharmacologically modulated by a clinically used antidepressant  
99 tianeptine (S 1574, [3-chloro-6-methyl-5, 5-dioxo-6,11-dihydro-(c,f)-dibenzo-(1,2-  
100 thiazepine)-11-yl) amino]-7 heptanoic acid), which restores impaired LTP in the  
101 stress/depression model <sup>32</sup>. As impaired synaptic plasticity is a common mechanism  
102 underlying both cognitive impairment and psychiatric disturbance such as anxiety and  
103 depression <sup>6,9,24,27,33</sup>, the major early-onset symptoms in HD <sup>1,2,34</sup>, here we have examined  
104 whether AMPAR surface diffusion is disturbed in HD models, how this is linked with  
105 impaired BDNF signaling and whether pharmacological modulation of AMPAR surface  
106 diffusion by tianeptine can serve as a promising therapeutic strategy to improve synaptic and  
107 memory dysfunction as well as anxiety/depression behavior in HD.

108

109

110

111

112

113

114 **RESULTS**

115 **Increased AMPAR surface diffusion in three different HD cellular models**

116 AMPARs are heteromeric proteins composed of different combinations of GluA1, GluA2,  
117 GluA3 or GluA4 subunits, in which GluA1-GluA2 di-heteromers are the most common  
118 combination in adult neurons. We thus first investigated endogenous GluA2-AMPAR surface  
119 diffusion using the single nanoparticle tracking approach in which a Quantum Dot (QD) is  
120 coupled to an antibody specific for the extracellular domain of the endogenous GluA2 subunit  
121 (Fig. 1a)<sup>32</sup>. We initially used rat primary hippocampal neuronal cultures transfected with  
122 exon1 mutant huntingtin which contains 69 polyglutamine expansion (exon1-polyQ-HTT),  
123 with exon1 wild-type huntingtin with 17 polyglutamine (exon1-wHTT) and empty vector as  
124 controls<sup>35</sup>. Compared to empty vector and exon1-wHTT, expression of exon1-polyQ-HTT  
125 significantly increased the surface diffusion of GluA2-AMPAR (Fig. 1b, c top panel). To  
126 avoid possible transfection artifacts, we next used primary hippocampal neurons from male  
127 R6/1 heterozygous transgenic mice, which overexpress the first exon of human HTT with 115  
128 polyQ and represent a fast model of HD. Only male HD mice were used throughout the paper  
129 in order to eliminate the possible influence of gender differences<sup>34</sup>. Similarly, an increase in  
130 GluA2-AMPARs surface diffusion was observed in neurons from R6/1 mice compared to WT  
131 littermate controls (Fig. 1d top panel). Furthermore, to circumvent overexpression artifacts  
132 and to better mimic the genetic situation in patients, we used neurons from male homozygous  
133 *Hdh*<sup>Q111/Q111</sup> knock-in mouse, in which polyQ repeats are directly engineered into the mouse  
134 HTT genomic locus and wHTT/polyQ-HTT is expressed at endogenous levels. Consistently,  
135 neurons from *Hdh*<sup>Q111/Q111</sup> knock-in mouse also displayed marked increase in GluA2 surface  
136 diffusion compared to WT littermates (Fig. 1e, top panel). These changes were partially due  
137 to a decreased fraction of immobile GluA2-AMPAR (surface diffusion  $\leq 0.01 \mu\text{m}^2/\text{s}$ ) (Fig.  
138 1c-e, bottom panels). Cumulative distributions of diffusion coefficients shift towards the right  
139 in the 3 HD models, indicating an increased GluA2-AMPAR surface diffusion.

140

141 As AMPARs are composed of different subunits, which can be differentially trafficked, we

142 also investigated the surface diffusion of the GluA1-AMPA population in the 4<sup>th</sup> cellular  
143 model of HD, in which full-length (FL) HTT with 75 polyQ and FL-wHTT with 17Q were  
144 overexpressed in rat hippocampal neurons. Similarly, the surface diffusion coefficients of  
145 GluA1-AMPA were markedly increased in neurons expressing FL-polyQ-HTT compared  
146 to neurons expressing FL-wHTT (Supplemental Fig. 1). Collectively, these data demonstrate  
147 in different complementary cellular models of HD that the surface diffusion of GluA2 and  
148 GluA1 subunits of AMPAR was markedly increased.

149

150 **Surface GluA2-AMPA failed to stabilize on the neuronal surface after chemical LTP**  
151 **(cLTP) induction in an HD cellular model**

152 The increased AMPAR surface diffusion in basal conditions prompted us to ask whether this  
153 could potentially lead to abnormal AMPAR surface stabilization during activity-dependent  
154 synaptic plasticity, such as LTP. Indeed, on the one hand, it has been shown that activity-  
155 dependent synaptic potentiation is associated with immobilization and subsequent  
156 accumulation of AMPARs at synapses<sup>31,36,37</sup>. On the other hand, polyQ expansion of HTT is  
157 associated with impaired LTP<sup>4-7</sup>. We thus examined AMPAR surface diffusion before and  
158 after three-minute cLTP stimuli<sup>38</sup> (300  $\mu$  M Glycine, 1  $\mu$  M Picrotoxin, without Mg<sup>2+</sup>) in rat  
159 hippocampal neurons overexpressing FL-wHTT or FL-polyQ-HTT using a super-resolution  
160 imaging method, Universal Point Accumulation Imaging in Nanoscale Topography (uPAINT)  
161<sup>39</sup>. uPAINT is not only able to generate super-resolved images but also provides dynamic  
162 information with large statistics revealing localization-specific diffusion properties of  
163 membrane biomolecules. Endogenous GluA2-AMPA were tracked with ATTO 647 labeled  
164 anti-extracellular GluA2 antibody and sorted into two groups according to their diffusion  
165 coefficient (immobile, Log (D)  $\leq$  -2; mobile, Log (D)  $>$  -2). In FL-wHTT-expressing  
166 neurons, we observed a decrease in the ratio of mobile to immobile AMPAR after cLTP  
167 stimuli relative to basal condition (Pre-LTP), reflecting an immobilization of surface  
168 AMPARs (Fig.2a). In contrast, the ratio of mobile to immobile AMPAR in FL-polyQ-HTT-

169 expressing neurons was not significantly different before and after LTP stimuli (Fig.2b).  
170 These data suggest that AMPARs fail to stabilize at the neuronal surface after LTP stimuli in  
171 HD models. This could explain, at least in part, the defects in the potentiation of AMPAR-  
172 mediated synaptic transmission in HD.

173

174 **Impaired BDNF-TrkB-CaMKII signaling through modulation of the interaction**  
175 **between stargazin and PSD95 contributes to the deregulation of AMPAR surface**  
176 **diffusion in the hippocampus**

177 BDNF is a prominent positive modulator of LTP<sup>13</sup>, which has been proposed to induce the  
178 delivery of AMPARs to the synapse under basal conditions<sup>40</sup>. However, it is not known  
179 whether and how AMPAR surface diffusion is modulated by BDNF signaling and whether it  
180 plays a role in HD pathogenesis. We thus asked if deficient BDNF signaling could account  
181 for the aberrant AMPAR surface diffusion in HD mouse models. We first characterized  
182 changes in the protein level of BDNF in HD mice. Consistent with a previous report<sup>6</sup>, using  
183 ELISA, we observed a significant decrease in the protein level of BDNF in the hippocampus  
184 of 10-week-old R6/1 and *Hdh*<sup>Q111/Q111</sup> mice compared to respective littermate controls (Fig.  
185 3b). We next studied BDNF intracellular transport in 3 complementary HD cellular models,  
186 as data on the BDNF intracellular transport in the hippocampus of HD mice are still lacking.  
187 Slower anterograde and retrograde BDNF intracellular transport was exhibited by neurons  
188 expressing polyQ-HTT relative to wHTT-expressing neurons (Fig.3c, 3d), and by R6/1 and  
189 *Hdh*<sup>Q111/Q111</sup> mouse hippocampal neurons compared to respective WT littermate controls (Fig.  
190 3e and 3f, respectively). Note that we observed slower BDNF velocity in neurites (Fig. 3d,  
191 3e) than in axons in hippocampal neurons (Fig. 3f), which is consistent with previous studies  
192 in cortical neurons<sup>41,42</sup>. Altogether, these data suggested that reduced BDNF protein  
193 production and impaired intracellular transport are common features to different categories of  
194 HD models.

195

196 Next we dissected the potential signaling mechanism by which BDNF modulates AMPAR

197 surface diffusion in HD models. BDNF is known to bind to TrkB receptors, leading to the  
198 activation of CaMKII<sup>13</sup>, which is critically required for the synaptic recruitment of AMPAR  
199 during both development and plasticity<sup>36</sup>. Active CaMKII phosphorylated at threonine 286  
200 (T286) is reported to be reduced in the hippocampus of *Hdh*<sup>Q111/Q111</sup> mouse models<sup>9</sup>. We next  
201 confirmed the decrease in CaMKII activity in a HD cellular model by co-transfecting rat  
202 hippocampal neurons with FL-wHTT/FL-polyQHTT and a fluorescence resonance energy  
203 transfer (FRET)-based CaMKII $\alpha$ , named REACH-CaMKII. The amino and carboxy termini  
204 of REACH-CaMKII are labeled with the FRET pair of monomeric enhanced green  
205 fluorescent protein (mEGFP) and resonance energy-accepting chromoprotein (REACH), a  
206 non-radiative yellow fluorescent protein variant<sup>43</sup>. The activation of REACH-CaMKII  
207 associated with T286 phosphorylation changes the conformation of CaMKII $\alpha$  to the open  
208 state in which its kinase domain is exposed, thereby decreasing FRET and increasing the  
209 fluorescence lifetime of mEGFP (Supplemental Fig. 2a). Rat hippocampal neurons  
210 transfected with GFP-PSD95 alone were used as negative control. GFP-PSD95-expressing  
211 cells showed high lifetime in both dendritic puncta and shaft indicating no FRET. FL-wHTT-  
212 and FL-polyQ-HTT-expressing cells both exhibited FRET revealed by shorter lifetime than  
213 GFP-PSD95-expressing cells, indicating activated CaMKII $\alpha$ . However, the REACH-  
214 CaMKII $\alpha$  lifetime in dendritic puncta (Supplemental Fig. 2c) and shaft (Supplemental Fig.  
215 2d) in FL-polyQ-HTT-expressing cells are significantly lower than in FL-wHTT-expressing  
216 cells, indicating stronger FRET and thus weaker CaMKII $\alpha$  activity.

217

218 We reasoned that if reduced CaMKII activity is responsible for aberrant AMPAR surface  
219 trafficking, then over-expression of constitutively active CaMKII should be able to rescue the  
220 FL-polyQ-HTT-induced increase in AMPAR surface diffusion. This is indeed what we  
221 observed (Fig. 3g). We assumed that if reduced CaMKII activity results from impaired  
222 BDNF-TrkB signaling pathway, then the application of exogenous BDNF should have similar  
223 effect. As expected, the application of exogenous BDNF similarly restored a lower GluA2-  
224 AMPAR surface diffusion (Fig. 3h, green bar). This rescue effect of BDNF requires the



225 activation of TrkB and CaMKII as this effect was completely blocked by the addition of the  
226 BDNF scavenger TrkB-Fc or CaMKII inhibitor kn93 (Fig. 3h, orange and red bar,  
227 respectively). This indicates that BDNF-TrkB-CamKII signaling pathway plays a key role in  
228 stabilizing surface AMPARs.

229

230 The CaMKII-induced AMPAR immobilization requires the AMPAR auxiliary subunit  
231 stargazin and its binding to scaffold proteins of the postsynaptic density, such as PSD-95<sup>32,36</sup>.

232 We thus examined the role of the interaction between stargazin and PSD-95 in mediating  
233 BDNF's effects by expressing  $\Delta$ C stargazin ( $\Delta$ C Stg), in which the interaction domain with  
234 PSD-95 was deleted. In  $\Delta$ C-Stg but not WT stargazin-expressing neurons, administration of  
235 BDNF failed to reduce GluA2-AMPA surface diffusion (Fig.3i). These data suggest that  
236 impaired BDNF-TrkB-CaMKII signaling via the interaction between stargazin and PSD95  
237 accounts for the disturbance of AMPAR surface diffusion in the hippocampus of HD models.

238

### 239 **Tianeptine improved BDNF protein production as well as intracellular trafficking in the** 240 **hippocampus of HD models**

241 BDNF is not a good candidate for HD treatment due to its instability and difficulties to cross  
242 the blood-brain barrier<sup>20,21,44</sup>. An alternative approach, therefore, is to elevate endogenous  
243 BDNF protein or trafficking using other exogenous agents. Our previous work showed that  
244 the anti-depressant tianeptine modulates AMPAR surface diffusion and improved LTP in  
245 stress/depression models<sup>32</sup>. It has also been reported that chronic tianeptine treatment  
246 increased BDNF protein level in various rodent brain structures<sup>45,46</sup>. However, the effect of  
247 tianeptine on BDNF intracellular trafficking is not known and it is unclear whether tianeptine  
248 modulates BDNF signaling in HD models. We thus examined the effect of tianeptine on  
249 BDNF protein production as well as intracellular trafficking in different HD models.  
250 Hippocampal BDNF protein production was evaluated using ELISA and Western Blot  
251 methods in R6/1 and *Hdh*<sup>Q111/Q111</sup> mice at 10-12 weeks of age. Because at this age, R6/1 and  
252 *Hdh*<sup>Q111/Q111</sup> mice were reported to show LTP defects and R6/1 mice gradually develop

253 cognitive deficits <sup>4,6</sup>. We found that the reduced hippocampal BDNF protein levels in R6/1  
254 (Fig. 4a-c) and in *Hdh*<sup>Q111/Q111</sup> mice (Fig. 4d) were both significantly improved by tianeptine  
255 administration (25mg/kg, i.p. daily for 4 days for R6/1 mice; and 10mg/kg, once for  
256 *Hdh*<sup>Q111/Q111</sup> mice). Note that a single tianeptine injection at 10mg/kg was inefficient for R6/1  
257 mice (data not shown), which may be due to the more severe phenotypes in this mouse model  
258 <sup>47</sup>. We next examined tianeptine effect on BDNF intracellular trafficking in 3 different HD  
259 cellular models. The application of tianeptine fully rescued the velocity of BDNF anterograde  
260 and retrograde transport in polyQ-HTT-expressing neurons (Fig. 4e, 4f) as well as in  
261 hippocampal neurons from R6/1 (Fig. 4g) and *Hdh*<sup>Q111/Q111</sup> mice (Fig.4h). In addition,  
262 tianeptine also augmented BDNF intracellular trafficking in WHTT-expressing neurons and  
263 in neurons from WT control for *Hdh*<sup>Q111/Q111</sup> mice (Supple Fig. 3). These data suggest that  
264 tianeptine regulates hippocampal BDNF signaling at least at 2 levels, namely BDNF protein  
265 production and intracellular transport.

266

### 267 **BDNF-TrkB signaling pathway mediates the tianeptine effect on BDNF intracellular** 268 **trafficking and AMPAR surface diffusion**

269 To further clarify the functional mechanism of tianeptine, we examined if the tianeptine-  
270 induced increase in BDNF intracellular trafficking could be prevented by a selective TrkB  
271 receptor inhibitor, Cyclotraxin-B (CB), which is a small inhibitor peptide mimicking the  
272 reverse turn structure of the variable region III that protrudes from the core of BDNF <sup>48</sup>.  
273 Indeed, tianeptine (50  $\mu$ M) induced improvement of anterograde and retrograde BDNF  
274 intracellular transport was fully blocked by pre-incubation with CB (1  $\mu$ M) (Fig 5a, b). This  
275 suggested that tianeptine's effect on BDNF intracellular trafficking is likely mediated through  
276 TrkB receptor. Since BDNF is not the sole ligand for TrkB receptor, we then postulated that if  
277 tianeptine influences BDNF intracellular trafficking through BDNF signaling rather than  
278 working in parallel, then addition of exogenous BDNF should be able to occlude tianeptine's  
279 effect. Indeed, the administration of BDNF (100ng/ml) similarly rescued the decreased BDNF  
280 intracellular trafficking induced by polyQ-HTT and the combination of BDNF and tianeptine

281 did not exhibit additive effect (Fig.5c). These data indicate that tianeptine affects BDNF  
282 intracellular trafficking possibly through BDNF-TrkB signaling pathway. We next asked  
283 whether tianeptine is also able to restore AMPAR surface traffic and if this effect is mediated  
284 by TrkB receptors. The application of tianeptine significantly slowed down AMPAR surface  
285 diffusion in polyQ-HTT-expressing neurons, an effect fully blocked by the TrkB receptor  
286 inhibitor Cyclothiazin-B and TrkB-Fc (Fig. 5 d, e). Collectively, these data suggest that the  
287 tianeptine effect on BDNF intracellular trafficking and AMPAR surface diffusion is mediated  
288 by BDNF-TrkB signaling pathway.

289

290 **Tianeptine enhanced the impaired hippocampal CA1 LTP and hippocampus-dependent**  
291 **memory as well as anxiety/depression-like behavior in complementary HD mouse**  
292 **models**

293 BDNF-TrkB signaling and AMPAR surface diffusion are critically involved in hippocampal  
294 plasticity and learning and memory<sup>13,23</sup>. We thus asked if tianeptine could rescue the  
295 impaired hippocampal LTP and hippocampal-dependent memory in 3 different mouse  
296 models of HD. Besides male heterozygous R6/1 transgenic mice and homozygous *Hdh*<sup>Q111/Q111</sup>  
297 knock-in mice, we employed a 3rd mouse model, male CAG140 heterozygous knock-in mice,  
298 for behavior test. Heterozygous mice are highly relevant to the disease, as the majority of HD  
299 patients are heterozygous<sup>3</sup>. In addition, CAG140 knock-in mice carry 140 polyQ and thus  
300 have earlier onset of symptoms than *Hdh*<sup>Q111/Q111</sup> knock-in mice. The fEPSPs were recorded from  
301 mouse hippocampal CA1 neurons (Fig. 6a,b). R6/1 transgenic mice and *Hdh*<sup>Q111/Q111</sup> knock-in  
302 mice were used at the age of 10-12 weeks. R6/1 mice showed a decrease in LTP of fEPSP  
303 slope compared to WT littermate control, which was partially rescued by chronic treatment of  
304 tianeptine at 25mg/kg (i.p. daily for 8 weeks) (Fig.6a) but not tianeptine at 10mg/kg (i.p. daily  
305 for 8 weeks)(data not shown). This suggested a dose-dependent effect of tianeptine. Very  
306 similar results were obtained in *Hdh*<sup>Q111/Q111</sup> mice, in which LTP defects were normalized by a  
307 single injection of tianeptine (10mg/kg) (Fig. 6b). The restorative effect of tianeptine on LTP  
308 in HD mice raises the question of whether it can also rescue HD-related hippocampus-

309 dependent cognitive impairments. In order to test early therapeutic intervention, we started to  
310 administer saline/tianeptine (10mg/kg, i.p. daily) to R6/1 and WT littermate mice from 4  
311 weeks of age, when the mice do not typically present with cognitive deficits<sup>4</sup>. At 12 weeks of  
312 age, the mice were subjected to open field test, Y-maze and contextual fear conditioning. The  
313 latter two tasks are hippocampal-dependent memory tasks<sup>49,50</sup>, respectively based on novelty  
314 attractiveness and associated threat<sup>51</sup>. Vehicle-treated R6/1 mice spent much less time in the  
315 novel arm than vehicle-treated WT mice, suggesting that R6/1 mice have impaired spatial  
316 working memory (Fig. 6c). Interestingly, tianeptine administration improved Y-maze  
317 performance of R6/1 mice, but not that of WT mice. This improvement is not due to a change  
318 in moving velocity, as vehicle- and tianeptine-treated R6/1 mice had similar moving velocity  
319 in open field (Supplemental Fig. 4a).

320

321 Contextual fear conditioning, assessed by measuring the freezing behavior a mouse typically  
322 exhibits when re-exposed to a context in which a mild foot shock was beforehand delivered,  
323 reflects hippocampal-dependent memory<sup>49</sup>. Vehicle-treated R6/1 mice exhibited less freezing  
324 in the contextual fear test compared to vehicle-treated WT littermates, indicating a worse  
325 memory, which was rescued by tianeptine treatment (Fig. 6d). Similarly, for the spatial  
326 working memory tested in Y-maze, no beneficial effect was observed on tianeptine-treated  
327 WT mice. We thus propose that tianeptine specifically rescued the hippocampal-dependent  
328 memory of R6/1 mice.

329

330 As HD mice also typically present an anxiety/depression-like phenotype<sup>47,52</sup>, we asked if  
331 chronic tianeptine treatment would attenuate anxiety/depression-like phenotype in CAG140  
332 heterozygous knock-in mice. The anxiety-like behavior of CAG140 mice was assessed using  
333 the Elevated Plus Maze (EPM) paradigm and Novelty Suppressed Feeding (NSF) paradigm.  
334 Anxiety-like phenotypes are characterized by decreased time spent in opened arms in EPM or  
335 an increase in latency to feed in NSF, which we observed in 6-month old CAG140 mice (data  
336 not shown). Here, we specifically investigated the early intervention therapy in HD and

337 treated CAG140 mice mice starting from 3 months of age, when the anxiety phenotype is not  
338 fully established (compared to 6 months old mice, data not shown), and tested at 4 months of  
339 age. We found that compared to vehicle-treated CAG140 mice, chronically tianeptine-treated  
340 CAG140 mice spent significantly more time in opened arms in EPM (Fig. 6e), while their  
341 locomotor activity revealed by ambulatory distance was not significantly affected  
342 (Supplemental Fig.4b left panel). The treatment also markedly decreased the latency to feed  
343 in NSF (Fig. 6f) without altering the home food consumption (Supplemental Fig.4b right  
344 panel). In contrast, tianeptine did not significantly alter the behavior of WT mice, suggesting  
345 that chronic tianeptine treatment also specifically improves the anxiety/depression-like  
346 behavior in HD mice.

347  
348  
349  
350  
351  
352  
353  
354  
355  
356  
357  
358  
359  
360  
361  
362  
363  
364  
365  
366  
367  
368  
369  
370  
371  
372  
373  
374  
375  
376  
377  
378  
379  
380  
381  
382  
383  
384

385

386

387 **DISCUSSION**

388 AMPAR surface diffusion plays a key role in the regulation of the AMPAR synaptic content

389 during glutamatergic synaptic plasticity<sup>22,30,31</sup>. AMPARs constantly switch on the neuronal

390 surface between mobile and immobile states driven by thermal agitation and reversible

391 binding to stable elements such as scaffold or cytoskeletal anchoring slots or extracellular

392 anchors. Even in synapses, AMPARs are not totally stable with around 50% of them moving

393 constantly by Brownian diffusion within the plasma membrane, promoting continuous

394 exchanges between synaptic and extrasynaptic sites<sup>22</sup>. This process is highly regulated by

395 neuronal activity and other stimuli. It has been shown that the majority of AMPARs

396 incorporated into synapses during LTP is from surface diffusion while exocytosed receptors

397 likely serve to replenish the extrasynaptic pool available for subsequent bouts of plasticity<sup>31</sup>.

398 This AMPAR redistribution followed by immobilization and accumulation of AMPARs at

399 synapses is the crucial step for the enhanced synaptic transmission during synaptic

400 potentiation<sup>31,36,37</sup>. In the present study, we provide the first direct proof in three

401 complementary HD models that AMPAR surface mobility is significantly increased and that

402 AMPARs fail to stabilize at the surface after cLTP stimuli. This opens a new perspective into

403 the molecular mechanism underlying the impaired hippocampal synaptic plasticity in HD. It

404 is noteworthy that disturbed AMPAR trafficking is also proposed to be one of the first

405 manifestations of synaptic dysfunction that underlies Alzheimer's Disease (AD)<sup>23,53,54</sup>, which

406 shares many clinical and pathological similarities with HD, such as early-onset cognitive

407 deficiency before perceptible neuronal degeneration. Together with our previous finding that

408 deregulated AMPAR surface diffusion underlies impaired LTP in stress/depression models<sup>28</sup>,

409 these lines of evidence indicate that dysregulation of AMPAR surface diffusion may represent

410 a common molecular basis for the impaired hippocampal synaptic plasticity and memory in

411 various neuronal disorders.

412

413 It is generally accepted that BDNF via interaction with TrkB receptors enhances synaptic

414 transmission and plasticity in adult synapses, while its binding to p75<sup>NTR</sup> has been  
415 demonstrated to negatively modulate synaptic plasticity, spine-dendrite morphology and  
416 complexity<sup>13</sup>. Recent studies show that impaired BDNF delivery, as well as the abnormally  
417 reduced expression of TrkB receptor and enhanced p75<sup>NTR</sup> expression account for the  
418 hippocampal synaptic and memory dysfunction<sup>9,18,19</sup>. The phosphorylation of GluA1 on Ser-  
419 831 through activation of protein kinase C and CaMKII via TrkB receptors has been proposed  
420 to be responsible for AMPAR synaptic delivery<sup>13</sup>. However, other evidence indicates that  
421 GluA1 phosphorylation at Ser-831 alters single-channel conductance rather than receptor  
422 anchoring<sup>55</sup>. Here we provide the first evidence in HD models that administration of BDNF  
423 slows down the increased AMPAR surface diffusion via interaction between PSD95 and  
424 stargazin, which is downstream of TrkB-CaMKII signaling pathway. It is possible that both  
425 processes, that is, change in the single-channel conductance and receptor anchoring (this  
426 study), occur in parallel and affect AMPAR signaling. Interestingly, the reduced CaMKII  
427 activity reported in *Hdh*<sup>Q111/Q111</sup> knock-in mice could be prevented by normalization of p75<sup>NTR</sup>  
428 levels<sup>9</sup>. This effect could be attributable to the preservation of TrkB signaling, as it has been  
429 shown that decreasing p75<sup>NTR</sup> expression or blocking its coupling to the small GTPase RhoA  
430 normalizes TrkB signaling; while upregulation of p75<sup>NTR</sup> signaling through phosphatase-and-  
431 tensin-homolog-deletedon-chromosome-10 (PTEN) results in impaired TrkB signaling<sup>19</sup>.  
432 Thus, impaired BDNF delivery and aberrant processing of BDNF signal may converge on  
433 TrkB-CaMKII signaling pathway affecting AMPAR surface diffusion.

434

435 Tianeptine is a well-tolerated antidepressant primarily used in the treatment of major  
436 depressive disorders<sup>56</sup>. It is structurally similar to a tricyclic antidepressant (TCA), but has  
437 different pharmacological properties than typical TCAs as it produces its antidepressant  
438 effects likely through the alteration of glutamate receptor activity<sup>32,56</sup>. Tianeptine alters  
439 glutamatergic transmission, increasing for instance the phosphorylation of GluA1 subunits<sup>57</sup>  
440 and activating CaMKII and protein kinase A via the p38, p42/44 mitogen-activated protein  
441 kinases (MAPK) and c-Jun N-terminal kinases (JNK) pathways<sup>58</sup>. Through unknown

442 mechanisms, tianeptine prevents stress-induced dendritic atrophy, improves neurogenesis,  
443 reduces apoptosis and normalizes metabolite levels and hippocampal volume<sup>56</sup>. In the present  
444 study, we show in complementary HD models that tianeptine restored AMPAR surface  
445 diffusion, via BDNF-TrkB signaling pathway, and rescued defective LTP and hippocampal-  
446 dependent memory. Interestingly, the activation of BDNF-TrkB signaling pathway is also  
447 required for the effect on the depression-like behavior of some typical antidepressants, such  
448 as fluoxetine and imipramine<sup>59,60</sup>. The mechanisms underlying chronic tianeptine treatment  
449 may involve BDNF-induced neurogenesis<sup>56</sup>, however, our finding that a single dose  
450 administration of tianeptine is sufficient to rescue aberrant LTP in *Hdh*<sup>Q111/Q111</sup> knock-in mice  
451 points to additional mechanisms. Given the critical role of AMPAR surface diffusion in  
452 hippocampal synaptic plasticity<sup>23,31,36,37</sup>, we argue that the beneficial effects of tianeptine on  
453 the impaired LTP and hippocampal-dependent memory stem, at least in part, from its  
454 normalization of AMPAR surface diffusion. Although tianeptine is also able to augment  
455 BDNF intracellular trafficking in WT controls (Supple Fig. 3) and immobilize AMPAR  
456 surface diffusion under basal conditions<sup>32</sup>, it did not significantly improve hippocampal-  
457 dependent memory in WT mice, suggesting that the maintenance of a physiological dynamic  
458 equilibrium is key to an effective treatment. The present study also showed beneficial effect  
459 of tianeptine on the anxiety/depression-like behavior in CAG140 knock-in mouse model.  
460 Note that cognitive dysfunction and psychiatric pathologies such as depression, stress and  
461 anxiety are typical features of HD, which occur well before the onset of motor dysfunction  
462<sup>1,2,34,61,62</sup>, thus the use of tianeptine may represent a promising early therapeutic strategy for  
463 HD targeting both psychiatric and cognitive defects. Moreover, that tianeptine is a clinically  
464 used drug will also facilitate clinical trials.

465

466 In conclusion, we unravel AMPAR surface diffusion as a potential novel therapeutic target  
467 for early intervention in HD and propose a new therapeutic strategy for HD using an  
468 antidepressant tianeptine, which improved hippocampal synaptic and memory deficits as well



469 as anxiety/depression-like behavior in HD mice possibly through the modulation of BDNF

470 signaling and AMPAR surface diffusion.

471

472 **MATERIALS AND METHODS**

473

474 **HD transgenic mice, primary Neuronal Cultures and transfection**

475 The heterozygous male R6/1 mice (Jackson Laboratory, Main Harbor, NY) were crossed with  
476 female C57BL/6 mice (Charles River, Lyon). Homozygous *Hdh*<sup>Q111/Q111</sup> KI mice of HD on  
477 CD1 background are generous gift from M.E. MacDonald<sup>63</sup>. The CAG140 are heterozygous  
478 mice with C57Bl6N/J background. The animals were housed with food and water ad libitum  
479 under a 12h light–dark cycle. All work involving animals was conducted according to the  
480 rules of ethics of the Committee of University of Bordeaux and the Aquitaine (France) and  
481 the Institutional Animal Care and Use Committee (European Directive, 2010/63/EU for the  
482 protection of laboratory animals, permissions # 92-256B, authorization ethical committee  
483 CEEA 26 2012\_100). Polymerase chain reaction (PCR) genotyping with DNA extracted from  
484 a piece of tail was carried to identify mice genotype.

485

486 Primary cultures of hippocampal neurons were prepared following a previously described  
487 method from (1) Sprague-Dawley rats at E18; (2) *Hdh*<sup>Q111/Q111</sup> KI mice and WT littermates at  
488 P0 for AMPAR surface tracking and *Hdh*<sup>Q111/Q111</sup> KI mice and WT mice at E15 for BDNF  
489 intracellular tracking; (3) R6/1 mice and WT littermates at P0<sup>10,64</sup>. Cells were plated at a  
490 density of 200 x 10<sup>3</sup> cells for rat culture and 450 x 10<sup>3</sup> cells for mice culture per 60 mm dish  
491 on poly-lysine pre-coated cover slips. Cultures were maintained in serum-free neurobasal  
492 medium (Invitrogen) and kept at 37 °C in 5% CO<sub>2</sub> for 20 div at maximum. Cells were  
493 transfected with appropriate plasmids using Effectene (Qiagen).

494

495 **Plasmid Constructs & Chemical product**

496 Homer 1C::GFP with CaMKII promoter was generated by subcloning homer 1C cDNA into  
497 the eukaryotic expression vector pcDNA3 (Invitrogen); EGFP was inserted at the N-terminus  
498 of the Homer 1C sequence. Exon1 mutant huntingtin contains 69 polyglutamine–expansion  
499 (exon1-polyQ-HTT) and wild-type huntingtin with 17 polyglutamine (exon1-wHTT)<sup>35</sup>. Full-

500 length HTT plasmids encode full-length huntingtin with 17 polyQ (FL-wHTT) or 75Q (FL-  
501 polyQ-HTT). 480-17Q, 480-68Q huntingtin plasmids encode the first 480 amino acids  
502 fragment of huntingtin with 17 (Nter-wHTT) or 68 glutamines (Nter-polyQ-HTT) <sup>65,66</sup>.  
503 Tianeptine was purchased from T & W group and MedChemexpress CO.,Ltd; BDNF from  
504 Sigma-Aldrich; TrkB-Fc from R&D Systems; kn93 from Tocris. Homemade Cyclotraxin-B  
505 and Cyclotraxin-B synthesized by Bio S&T were used.

506

### 507 **Cyclotraxin B synthesis**

508 Cyclotraxin B was synthesized at a 0.05 mmol scale. Amino acids were assembled by  
509 automated microwave solid phase peptide synthesis on a CEM microwave-assisted Liberty-1  
510 synthesizer following the standard coupling protocols provided by the manufacturer.  
511 Methionine was replaced by Norleucine ( $\lambda$ ), a more stable isostere. Linear peptide was  
512 cleaved (TFA:H<sub>2</sub>O:EDT:TIS, 94:2.5:2.5:1) and purified by HPLC. Disulfide bond formation  
513 was carried out for 10 hrs in H<sub>2</sub>O in the presence of DMSO (5%) and ammonium acetate  
514 (0.05 M) at high dilution of the peptide (100  $\mu$ M). Solvent excess was removed and the  
515 peptide was purified by RP-HPLC (YMC C18, ODS-A 5/120, 250x20 mm, UV detection at  
516 228 and 280 nm, using a standard gradient: 5% MeCN containing 0.1% TFA for 5 min  
517 followed by a gradient from 10 to 40% over 40 min in dH<sub>2</sub>O containing 0.1% TFA at a flow  
518 rate of 12 mL.min<sup>-1</sup>). Peptides were characterized by analytic RP-HPLC and MALDI.  
519 Peptides were quantified by absorbance measurement at 280 nm, aliquoted, lyophilized and  
520 stored at -80 °C until usage.

521

### 522 **Single nanoparticle (Quantum dot) tracking and surface diffusion calculation**

523 Rat primary hippocampal neurons were co-transfected at DIV 10-11 with GFP/homer1c-GFP  
524 and wHTT/polyQ-HTT at the ratio of 1:9 to ensure that the majority of GFP-transfected  
525 neurons were transfected with HTT. Homer1c was used as a postsynaptic marker.  
526 Endogenous GluA2 and GluA1 quantum dot (QD) tracking was performed at DIV 11-12 as  
527 previously described <sup>32</sup>. Neurons were first incubated with mouse monoclonal antibody

528 against N-terminal extracellular domain GluA2 subunit (a kind gift from E. Gouaux, Oregon  
529 Health and Science University, USA) or rabbit polyclonal antibody against N-terminal  
530 extracellular domain GluA1 subunit (PC246, Calbiochem) followed incubation with QD 655  
531 Goat F(ab')<sub>2</sub> anti-mouse or anti-Rabbit IgG (Invitrogen). Non-specific binding was blocked  
532 by 5% BSA (Sigma-Aldrich). QDs were detected by using a mercury lamp and appropriate  
533 excitation/emission filters. Images were obtained with an interval of 50 ms and up to 1000  
534 consecutive frames. Signals were detected using a CCD camera (Quantem, Roper Scientific).  
535 QDs were followed on randomly selected dendritic regions for up to 20 min. QD recording  
536 sessions were processed with the Metamorph software (Universal Imaging Corp). The  
537 instantaneous diffusion coefficient,  $D$ , was calculated for each trajectory, from linear fits of  
538 the first 4 points of the mean-square-displacement versus time function using  $MSD(t) = \langle r^2 \rangle$   
539  $(t) = 4Dt$ . The two-dimensional trajectories of single molecules in the plane of focus were  
540 constructed by correlation analysis between consecutive images using a Vogel algorithm.  
541 QD-based trajectories were considered synaptic if colocalized with Homer 1C dendritic  
542 clusters for at least five frames.

543

#### 544 **BDNF intracellular transport**

545 Rat hippocampal neurons were co-transfected at DIV 9-10 with GFP-fused 480-17Q  
546 (GFP::Nter-wHTT) or 480-68Q (GFP::Nter-polyQ-HTT) and mCherry-BDNF at the ratio of  
547 4:1 using Effectene (QIAGEN). Live imaging was carried out at DIV 10-11. The movement  
548 of BDNF-containing vesicles was tracked using video-microscopy on an inverted Leica DMI  
549 6000 Year microscope (Leica Microsystems, Wetzlar, Germany) equipped with a HQ2  
550 camera (Photometrics, Tucson, USA). The objective HCX PL used was a CS APO 63X NA  
551 1.32 oil. The atmosphere was 37 °C incubator created with year box and air heating system  
552 (Life Imaging Services, Basel, Switzerland). Acquisitions and calculation were done on the  
553 MetaMorph software (Molecular Devices, Sunnyvale, USA). For BDNF axonal trafficking in  
554 hippocampal neurons of mouse *Hdh*<sup>Q111/Q111</sup> KI and WT mice, hippocampal neurons at E15  
555 were used. Microchambers, neuronal transfection as well as videomicroscopy were previously

556 described<sup>42</sup>. Images were collected in stream mode using a Micromax camera (Roper  
557 Scientific) with an exposure time of 100 to 150 ms. Projections, animations and analyses were  
558 generated using ImageJ software (<http://rsb.info.nih.gov/ij/>, NIH, USA). Maximal projection  
559 was performed to identify the vesicles paths, which in our system corresponds to vesicle  
560 movements in axons. Kymographs and analyses were generated with the KymoToolBox, a  
561 home-made plug-in<sup>42</sup>.

562

### 563 **UPAINT**

564 Rat primary hippocampal neurons were co-transfected at DIV 4 with homer1c-GFP and FL-  
565 wHTT/polyQ-HTT for 2 weeks. Homer1c was used as a postsynaptic marker. Single-  
566 molecule fluorescent spots were localized in each frame and tracked over time as previously  
567 described<sup>39</sup>.

568

### 569 **BDNF enzyme-linked immunosorbent assay (ELISA)**

570 The BDNF concentration was evaluated using BDNF ELISA Kit (Millipore, Abnova).

571

### 572 **Fluorescence Resonance Energy Transfer (FRET)- Fluorescence-lifetime imaging** 573 **microscopy (FLIM) experiments**

574 A FRET-based CamKII $\alpha$ , named REACh-CamKII is a kind gift from R. Yasuda (Max Planck  
575 Institute, Florida, USA). The amino and carboxy termini of CamKII $\alpha$  are labeled with the  
576 FRET pair of monomeric enhanced green fluorescent protein (mEGFP) and resonance  
577 energy-accepting chromoprotein (REACh), a non-radiative yellow fluorescent protein variant.  
578<sup>43,67</sup> FLIM experiments were performed at 37 °C using an incubator box with an air heater  
579 system (Life Imaging Services) installed on an inverted Leica DMI6000B (Leica  
580 Microsystem) spinning disk microscope and using the LIFA frequency domain lifetime  
581 attachment (Lambert Instruments, Roden, The Netherlands) and the LI-FLIM software. Cells  
582 were imaged with an HCX PL Apo X 100 oil NA 1.4 objective using an appropriate GFP  
583 filter set. Cells were excited using a sinusoidally modulated 1-W 477nm LED (lightemitting

584 diode) at 40 MHz under wild-field illumination. Emission was collected using an intensified  
585 CCD LI2CAM camera (FAICM; Lambert Instruments). The phase and modulation were  
586 determined from a set of 12 phase settings using the manufacturer's LI-FLIM software.  
587 Lifetimes were referenced to a 1 $\mu$ M solution of fluorescein in Tris-HCl (pH 10) that was  
588 set at 4.00 ns lifetime. Signals were recorded with a back-illuminated Evolve EMCCD  
589 camera (Photometrics). Acquisitions were carried out on the software MetaMorph (Molecular  
590 Devices).

591

### 592 **Western blotting**

593 Western Blot is performed as previously described<sup>32</sup>. 10  $\mu$ g of protein was loaded per lane  
594 and analyzed by SDS-PAGE. Primary antibodies anti-BDNF antibody (Santa Cruz  
595 Biotechnology, sc-546); anti-Tubulin antibody (Sigma-Aldrich) were used.

596

### 597 **Ex vivo extracellular recording from hippocampal CA1 pyramidal neurons**

598 Male heterozygous R6/1 mice, *Hdh*<sup>Q111/Q111</sup> KI mice and respective WT littermates were used  
599 for ex vivo extracellular recording. *Hdh*<sup>Q111/Q111</sup> KI mice (10-12 week of age) received a single  
600 injection of tianeptine (i.p., 10mg/kg) with saline as negative control; R6/1 mice received  
601 chronic tianeptine treatment (25mg/kg, i.p. daily) starting from 4 weeks of age until 12 weeks  
602 of age. As described previously<sup>32</sup>, a hippocampal slice was transferred to a superfusing  
603 recording chamber with temperature controlled at 33.5 °C, and continuously perfused with  
604 oxygenated ACSF using a peristaltic pump (Ismatec, Switzerland). A teflon-coated tungsten  
605 bipolar stimulating electrode (Phymep, Paris, France) was positioned in stratum radiatum,  
606 allowing the afferent schaffer collateral-commissural pathway from the CA3 area to the CA1  
607 region to be stimulated. The field-EPSPs (fEPSPs) were recorded from stratum radiatum of  
608 CA1 area, using a glass electrode (3–5 M $\Omega$ ) pulled from borosilicate glass tubing (Havard  
609 Apparatus, USA; 1.5 mm O.D x 1.17 mm I.D) and filled with ACSF. Pulses were delivered at  
610 7.5s by a stimulus isolator (Isoflex, AMPI, Jerusalem, Israel), with adjusting current intensity  
611 to obtain 30-40 % of the maximum fEPSP. A theta-burst stimulation (TBS) protocol (4 pulses,

612 respectively, delivered at 100 Hz, repeated 10 times, at an interval of 200 ms) was delivered  
613 by Clampex10.4 (Molecular Devices, USA) and the stimulus isolator to induce LTP.  
614 Recordings were made continually for more than 60 min, following the TBS. Data were  
615 recorded with a Multiclamp700B (Axon Instruments, USA) and acquired with Clampex10.4.  
616 The slope of the fEPSP was measured using clampfit10.4 software, with all values  
617 normalized to a 5 min baseline period; the values during 50-60 min after TBS are reported in  
618 the figures as  $\pm$  standard error of the mean (SEM). Mean values were compared between  
619 genotypes and treatments using either unpaired Student's t-test as appropriate. The  
620 experiments were done blindly.

621

### 622 **Behavioral tests**

623 Male R6/1 and WT littermate mice were used for behavioral tests. At 4 weeks of age,  
624 littermate mice with mixed genotypes were housed (3-5 per cage) in polycarbonate standard  
625 cages (33x15x14cm) and randomly allocated to vehicle or drug treatment groups. Mice  
626 received daily intraperitoneal injection (i.p.) of 0.9% saline (vehicle) or tianeptine (10mg/kg)  
627 dissolved in 0.9% saline until 12 weeks of age, when the animals were subjected to a battery  
628 of behavioral tests. On day 1, all mice were subjected to Open Field test; on day 2, spatial  
629 memory was assessed in Y maze. Following a week rest, on day 9, a subset of mice were  
630 further tested for contextual fear conditioning, which is performed lastly in order to minimize  
631 confounding factors. All behavioral testing was carried out in the light phase (light intensity:  
632 45-50 lux). Before each behavioral test, mice were individually housed in standard cages with  
633 sawdust, food and water and left undisturbed in the experimental room at least 30min before  
634 testing began.

635

### 636 **Open field**

637 The apparatus constituted of a white square arena (42cm x 42cm x 20 cm). Each animal was  
638 placed in the center of the arena and allowed to explore for 20 min. Images tracked from a  
639 camera above the maze were analyzed with Ethovision (version 9.1). The total distance

640 traveled and the time spent moving were analyzed as readouts of locomotor activity. The  
641 apparatus was cleaned by ethanol 70% between mice.

642

### 643 **Y-maze**

644 Hippocampal-dependent spatial working memory was evaluated using Y-maze. The apparatus  
645 consisted of three identical grey plastic arms (42 x 8 x 15 cm) and spaced at 120° of each  
646 other. The maze was located in the middle of a room containing a variety of extramaze cues.  
647 A digital camera was mounted above the maze transmitting the data to a PC running the  
648 Ethovision system. Mice were assigned two arms (start and familiar arm) to which they were  
649 exposed during the first phase of the test (sample phase). The remaining third arm blocked by  
650 a gray plastic door constituted the novel arm during the second phase (test phase). Mice were  
651 placed at the end of the start arm and allowed to explore freely both the start and the other  
652 unblocked arm for 5 min before being removed from the maze and returned to the waiting  
653 cage. After 10 min in the waiting cage, the test phase began. During this phase, the door was  
654 removed and all three arms were unblocked; mice were placed at the end of the start arm and  
655 allowed to explore the entire maze for 2 min. Timing of both the sample and test phase  
656 periods began once the mouse had left the start arm. The apparatus was cleaned between the  
657 two phases in order to avoid olfactory cues. Time spent in the novel arm in comparison to  
658 time in all three arms was used as one readout for hippocampal-dependent spatial memory.

659

### 660 **Contextual fear conditioning**

661 Contextual fear conditioning provides a measure of memory by assessing a memory for the  
662 association between mild foot shock and a salient environmental cue. In the fear conditioning  
663 test, freezing behavior is defined as the complete lack of movement, which is a characteristic  
664 fear response in rodents, providing a readout of hippocampal-dependent memory. Fear  
665 conditioning was performed in a testing chamber with internal dimensions of 25 X 25 X 25  
666 cm, which has transparent plastic walls each side and steel bars on the floor. A camera  
667 mounted at one side recorded each session. The chamber was located inside a larger,



668 insulated, transparent plastic cabinet (67 X 53 X 55 cm) that provided protection from outside  
669 noise. The cabinet contained a ventilation fan that was operated during the sessions. Mice  
670 were held outside the experimental room in individual cages prior to testing. Training  
671 chambers were cleaned with 100% ethanol solution before and after each trial to avoid any  
672 olfactory cues. The experiments ran over two consecutive days. On Day 1, mice were placed  
673 in the conditioning chamber and 2 min 28s later received one footstock (2 s, 0.3 mA). Mice  
674 were removed from the chamber 30 s after the shock. On Day 2, they returned to the same  
675 conditioning chamber for a 3-min period in the exact same conditions as Day 1, but without  
676 electrical shock, to evaluate context-induced freezing.

677

#### 678 **Elevated plus maze (EPM)**

679 Male CAG140 heterozygous knock-in mice received daily i.p. injection of saline or tianeptine  
680 at 10mg/kg at 12 weeks of age. Behavioral tests were performed at 16 week of age. Each  
681 animal, over a week, was successively tested in the Elevated Plus Maze (EPM) and Novelty  
682 Suppressed Feeding (NSF), which represent different anxiety and depression behavior  
683 paradigms. Behavioral tests were performed during the light phase between 0700 and 1900.  
684 EPM was performed as previously<sup>68</sup>. The maze is a plus-cross-shaped apparatus, with two  
685 open arms and two arms closed by walls linked by a central platform 50 cm above the floor.  
686 Mice were individually put in the center of the maze facing an open arm and were allowed to  
687 explore the maze during 5 min. The time spent in and the number of entries into the open  
688 arms were used as an anxiety index. Locomotion was also measured to ensure any  
689 confounding effects. All parameters were measured using a videotracker (EPM3C, Bioseb,  
690 Vitrolles, France).

691

#### 692 **Novelty-Suppressed-Feeding (NSF)**

693 The NSF is a conflict test that elicits competing motivations: the drive to eat and the fear of  
694 venturing into the center of a brightly lit arena. The latency to begin to eat is used as an index  
695 of anxiety/depression-like behavior, because classical anxiolytic drugs as well as chronic

696 antidepressants decrease this measure. The NSF test was carried out during a 15-min period  
697 as previously described<sup>68</sup>. Briefly, the testing apparatus consisted of a plastic box (50x50x20  
698 cm), the floor of which was covered with approximately 2 cm of wooden bedding. Twenty-  
699 four hours prior to behavioral testing, all food was removed from the home cage. At the time  
700 of testing, a single pellet of food (regular chow) was placed on a white paper platform  
701 positioned in the center of the box. Each animal was placed in a corner of the box, and a  
702 stopwatch was immediately started. The latency to eat (defined as the mouse sitting on its  
703 haunches and biting the pellet with the use of forepaws) was timed. Immediately afterwards,  
704 the animal was transferred to its home cage, and the amount of food consumed by the mouse  
705 in the subsequent 5 min was measured, serving as a control for change in appetite as a  
706 possible confounding factor.

707

## 708 **Statistics**

709 For imaging data, statistical values are given as mean  $\pm$  SEM, or medians  $\pm$  interquartile  
710 range (IQR) defined as the interval between 25% - 75% percentile. Statistical significances  
711 were tested using Prism 6.0 (GraphPad, USA). Normally distributed data sets were compared  
712 using the paired or unpaired Student's *t*-test. Statistical significance between more than two  
713 normally distributed datasets was tested by one way ANOVA variance test followed by a  
714 Bonferroni test to compare individual pairs of data. Non-Gaussian data sets were tested by  
715 non-parametric Mann-Whitney test. For behavioral tests, statistical analysis was carried out  
716 by two-way ANNOVA with genotype and treatment as the between-subject factors.  
717 Indications of significance correspond to *p* values  $< 0.05$  (\*),  $p < 0.01$  (\*\*) and  $p < 0.001$   
718 (\*\*\*).

719

## 720 **ACKNOWLEDGMENTS**

721 We acknowledge E. Gouaux for the anti-GluA2 antibody; J.B. Sibarita for providing single  
722 particle analysis software; C Poujol, S Marais, F Cordelieres from Bordeaux Imaging Center,  
723 part of the France BioImaging national infrastructure, for support in microscopy; and C.

724 Breillat, E. Verdier, N Retailleau for cell culture and plasmid production. The guidance of  
725 Françoise Coussen for biochemistry is acknowledged. We thank Jia-Yi Li for valuable input  
726 in the early phase of this project. This work was supported by funding from the Conseil  
727 Régional d'Aquitaine, ANR NanoDom and Stim-Traf-Park, Labex BRAIN and ANR-10-  
728 INBS-04 France-BioImaging, Centre National de la Recherche Scientifique, ERC grant  
729 nanodyn-syn and ADOS to D.C. and Aquitaine Science Transfer grant to D.C and H.Z. and  
730 FRM to H.Z.

731

732

### 733 **AUTHOR CONTRIBUTIONS**

734 H.Z. performed AMPAR and BDNF trafficking as well as live cell imaging studies, C.Z.  
735 performed electrophysiological experiments, J.V. conducted biochemical studies and  
736 behavioral test in R6/1 mouse line and assisted in imaging analysis, D.Z. performed BDNF  
737 trafficking studies in *Hdh*<sup>Q111/Q111</sup> mouse neurons, D.J.D and C.B. conducted behavioral test in  
738 CAG140 mouse line; D.J.D also contributes to the interpretation of behavioral tests in  
739 CAG140 mouse line; M.S. and D.G. synthesized Cyclotraxin-B; Y.C contributed to  
740 supervision and interpretation of behavioral studies in R6/1 mouse line, F.S contributed to the  
741 supervision and interpretation of BDNF trafficking studies in *Hdh*<sup>Q111/Q111</sup> mouse neurons and  
742 behavioral tests in CAG140 mouse line, Y.H. contributed to the supervision of  
743 electrophysiology studies and format of all figures. D.C. and H.Z. developed the concept,  
744 supervised the project, contributed to the design and interpretation of all experiments, and  
745 wrote the manuscript. All authors had the opportunity to discuss results and comment on the  
746 manuscript.

### 747 **COMPETING FINANCIAL INTERESTS**

748

749 The authors declare no competing financial interests.

750

751

752

## References

753

- 754 1. Berrios, G.E., *et al.* Psychiatric symptoms in neurologically asymptomatic  
755 Huntington's disease gene carriers: a comparison with gene negative at  
756 risk subjects. *Acta Psychiatr Scand* **105**, 224-230 (2002).
- 757 2. Tabrizi, S.J., *et al.* Biological and clinical changes in premanifest and early  
758 stage Huntington's disease in the TRACK-HD study: the 12-month  
759 longitudinal analysis. *Lancet Neurol* **10**, 31-42 (2011).
- 760 3. Saudou, F. & Humbert, S. The Biology of Huntingtin. *Neuron* **89**, 910-926  
761 (2016).
- 762 4. Giralt, A., *et al.* Brain-derived neurotrophic factor modulates the severity  
763 of cognitive alterations induced by mutant huntingtin: involvement of  
764 phospholipaseCgamma activity and glutamate receptor expression.  
765 *Neuroscience* **158**, 1234-1250 (2009).
- 766 5. Hodgson, J.G., *et al.* A YAC mouse model for Huntington's disease with full-  
767 length mutant huntingtin, cytoplasmic toxicity, and selective striatal  
768 neurodegeneration. *Neuron* **23**, 181-192 (1999).
- 769 6. Lynch, G., *et al.* Brain-derived neurotrophic factor restores synaptic  
770 plasticity in a knock-in mouse model of Huntington's disease. *J Neurosci*  
771 **27**, 4424-4434 (2007).
- 772 7. Murphy, K.P., *et al.* Abnormal synaptic plasticity and impaired spatial  
773 cognition in mice transgenic for exon 1 of the human Huntington's disease  
774 mutation. *J Neurosci* **20**, 5115-5123 (2000).
- 775 8. Milnerwood, A.J., *et al.* Early development of aberrant synaptic plasticity  
776 in a mouse model of Huntington's disease. *Hum Mol Genet* **15**, 1690-1703  
777 (2006).
- 778 9. Brito, V., *et al.* Neurotrophin receptor p75(NTR) mediates Huntington's  
779 disease-associated synaptic and memory dysfunction. *J Clin Invest* **124**,  
780 4411-4428 (2014).
- 781 10. Zhang, H., *et al.* NGF rescues hippocampal cholinergic neuronal markers,  
782 restores neurogenesis, and improves the spatial working memory in a  
783 mouse model of Huntington's Disease. *J Huntingtons Dis* **2**, 69-82 (2013).
- 784 11. Chan, A.W., *et al.* A two years longitudinal study of a transgenic  
785 Huntington disease monkey. *BMC Neurosci* **15**, 36 (2014).
- 786 12. Majerova, V., *et al.* Disturbance of real space navigation in moderately  
787 advanced but not in early Huntington's disease. *J Neurol Sci* **312**, 86-91  
788 (2012).
- 789 13. Park, H. & Poo, M.M. Neurotrophin regulation of neural circuit  
790 development and function. *Nat Rev Neurosci* **14**, 7-23 (2013).
- 791 14. Zuccato, C., *et al.* Loss of huntingtin-mediated BDNF gene transcription in  
792 Huntington's disease. *Science* **293**, 493-498 (2001).
- 793 15. Mo, C., *et al.* High stress hormone levels accelerate the onset of memory  
794 deficits in male Huntington's disease mice. *Neurobiol Dis* **69**, 248-262  
795 (2014).
- 796 16. Simmons, D.A., *et al.* A small molecule TrkB ligand reduces motor  
797 impairment and neuropathology in R6/2 and BACHD mouse models of  
798 Huntington's disease. *J Neurosci* **33**, 18712-18727 (2013).

- 799 17. Brito, V., *et al.* Imbalance of p75(NTR)/TrkB protein expression in  
800 Huntington's disease: implication for neuroprotective therapies. *Cell*  
801 *Death Dis* **4**, e595 (2013).
- 802 18. Parsons, M.P. & Raymond, L.A. It's not necessarily all about the delivery in  
803 Huntington's disease. *Neuron* **83**, 6-8 (2014).
- 804 19. Plotkin, J.L., *et al.* Impaired TrkB receptor signaling underlies  
805 corticostriatal dysfunction in Huntington's disease. *Neuron* **83**, 178-188  
806 (2014).
- 807 20. Simmons, D.A., *et al.* Up-regulating BDNF with an ampakine rescues  
808 synaptic plasticity and memory in Huntington's disease knockin mice.  
809 *Proc Natl Acad Sci U S A* **106**, 4906-4911 (2009).
- 810 21. Nitta, A., *et al.* 4-methylcatechol increases brain-derived neurotrophic  
811 factor content and mRNA expression in cultured brain cells and in rat  
812 brain in vivo. *J Pharmacol Exp Ther* **291**, 1276-1283 (1999).
- 813 22. Choquet, D. & Triller, A. The dynamic synapse. *Neuron* **80**, 691-703  
814 (2013).
- 815 23. Shepherd, J.D. & Huganir, R.L. The cell biology of synaptic plasticity: AMPA  
816 receptor trafficking. *Annu Rev Cell Dev Biol* **23**, 613-643 (2007).
- 817 24. Volk, L., Chiu, S.L., Sharma, K. & Huganir, R.L. Glutamate synapses in  
818 human cognitive disorders. *Annu Rev Neurosci* **38**, 127-149 (2015).
- 819 25. Kessels, H.W. & Malinow, R. Synaptic AMPA receptor plasticity and  
820 behavior. *Neuron* **61**, 340-350 (2009).
- 821 26. Hu, H., *et al.* Emotion enhances learning via norepinephrine regulation of  
822 AMPA-receptor trafficking. *Cell* **131**, 160-173 (2007).
- 823 27. Krugers, H.J., Hoogenraad, C.C. & Groc, L. Stress hormones and AMPA  
824 receptor trafficking in synaptic plasticity and memory. *Nat Rev Neurosci*  
825 **11**, 675-681 (2010).
- 826 28. Groc, L., Choquet, D. & Chaouloff, F. The stress hormone corticosterone  
827 conditions AMPAR surface trafficking and synaptic potentiation. *Nat*  
828 *Neurosci* **11**, 868-870 (2008).
- 829 29. Huganir, R.L. & Nicoll, R.A. AMPARs and synaptic plasticity: the last 25  
830 years. *Neuron* **80**, 704-717 (2013).
- 831 30. Borgdorff, A.J. & Choquet, D. Regulation of AMPA receptor lateral  
832 movements. *Nature* **417**, 649-653 (2002).
- 833 31. Makino, H. & Malinow, R. AMPA receptor incorporation into synapses  
834 during LTP: the role of lateral movement and exocytosis. *Neuron* **64**, 381-  
835 390 (2009).
- 836 32. Zhang, H., *et al.* Regulation of AMPA receptor surface trafficking and  
837 synaptic plasticity by a cognitive enhancer and antidepressant molecule.  
838 *Mol Psychiatry* **18**, 471-484 (2013).
- 839 33. Duman, R.S., Aghajanian, G.K., Sanacora, G. & Krystal, J.H. Synaptic  
840 plasticity and depression: new insights from stress and rapid-acting  
841 antidepressants. *Nat Med* **22**, 238-249 (2016).
- 842 34. Pla, P., Orvoen, S., Saudou, F., David, D.J. & Humbert, S. Mood disorders in  
843 Huntington's disease: from behavior to cellular and molecular  
844 mechanisms. *Front Behav Neurosci* **8**, 135 (2014).
- 845 35. Saudou, F., Finkbeiner, S., Devys, D. & Greenberg, M.E. Huntingtin acts in  
846 the nucleus to induce apoptosis but death does not correlate with the  
847 formation of intranuclear inclusions. *Cell* **95**, 55-66 (1998).

- 848 36. Opazo, P., *et al.* CaMKII triggers the diffusional trapping of surface  
849 AMPARs through phosphorylation of stargazin. *Neuron* **67**, 239-252  
850 (2010).
- 851 37. Petrini, E.M., *et al.* Endocytic trafficking and recycling maintain a pool of  
852 mobile surface AMPA receptors required for synaptic potentiation.  
853 *Neuron* **63**, 92-105 (2009).
- 854 38. Lu, W., *et al.* Activation of synaptic NMDA receptors induces membrane  
855 insertion of new AMPA receptors and LTP in cultured hippocampal  
856 neurons. *Neuron* **29**, 243-254 (2001).
- 857 39. Constals, A., *et al.* Glutamate-induced AMPA receptor desensitization  
858 increases their mobility and modulates short-term plasticity through  
859 unbinding from Stargazin. *Neuron* **85**, 787-803 (2015).
- 860 40. Caldeira, M.V., *et al.* Brain-derived neurotrophic factor regulates the  
861 expression and synaptic delivery of alpha-amino-3-hydroxy-5-methyl-4-  
862 isoxazole propionic acid receptor subunits in hippocampal neurons. *J Biol*  
863 *Chem* **282**, 12619-12628 (2007).
- 864 41. Gauthier, L.R., *et al.* Huntingtin controls neurotrophic support and  
865 survival of neurons by enhancing BDNF vesicular transport along  
866 microtubules. *Cell* **118**, 127-138 (2004).
- 867 42. Zala, D., *et al.* Vesicular glycolysis provides on-board energy for fast  
868 axonal transport. *Cell* **152**, 479-491 (2013).
- 869 43. Lee, S.J., Escobedo-Lozoya, Y., Szatmari, E.M. & Yasuda, R. Activation of  
870 CaMKII in single dendritic spines during long-term potentiation. *Nature*  
871 **458**, 299-304 (2009).
- 872 44. Massa, S.M., *et al.* Small molecule BDNF mimetics activate TrkB signaling  
873 and prevent neuronal degeneration in rodents. *J Clin Invest* **120**, 1774-  
874 1785 (2010).
- 875 45. Reagan, L.P., *et al.* Tianeptine increases brain-derived neurotrophic factor  
876 expression in the rat amygdala. *Eur J Pharmacol* **565**, 68-75 (2007).
- 877 46. Zoladz, P.R., Park, C.R., Munoz, C., Fleshner, M. & Diamond, D.M.  
878 Tianeptine: an antidepressant with memory-protective properties. *Curr*  
879 *Neuropharmacol* **6**, 311-321 (2008).
- 880 47. Menalled, L., *et al.* Systematic behavioral evaluation of Huntington's  
881 disease transgenic and knock-in mouse models. *Neurobiol Dis* **35**, 319-  
882 336 (2009).
- 883 48. Cazorla, M., *et al.* Cyclotraxin-B, the first highly potent and selective TrkB  
884 inhibitor, has anxiolytic properties in mice. *PLoS One* **5**, e9777 (2010).
- 885 49. Maren, S., Aharonov, G. & Fanselow, M.S. Neurotoxic lesions of the dorsal  
886 hippocampus and Pavlovian fear conditioning in rats. *Behav Brain Res* **88**,  
887 261-274 (1997).
- 888 50. Morris, R.G., Garrud, P., Rawlins, J.N. & O'Keefe, J. Place navigation  
889 impaired in rats with hippocampal lesions. *Nature* **297**, 681-683 (1982).
- 890 51. LeDoux, J.E. Evolution of human emotion: a view through fear. *Prog Brain*  
891 *Res* **195**, 431-442 (2012).
- 892 52. Menalled, L.B., Sison, J.D., Dragatsis, I., Zeitlin, S. & Chesselet, M.F. Time  
893 course of early motor and neuropathological anomalies in a knock-in  
894 mouse model of Huntington's disease with 140 CAG repeats. *J Comp*  
895 *Neurol* **465**, 11-26 (2003).



- 896 53. Hsieh, H., *et al.* AMPAR removal underlies Abeta-induced synaptic  
897 depression and dendritic spine loss. *Neuron* **52**, 831-843 (2006).
- 898 54. Selkoe, D.J. Alzheimer's disease is a synaptic failure. *Science* **298**, 789-791  
899 (2002).
- 900 55. Hayashi, Y., *et al.* Driving AMPA receptors into synapses by LTP and  
901 CaMKII: requirement for GluR1 and PDZ domain interaction. *Science* **287**,  
902 2262-2267 (2000).
- 903 56. McEwen, B.S., *et al.* The neurobiological properties of tianeptine  
904 (Stablon): from monoamine hypothesis to glutamatergic modulation. *Mol*  
905 *Psychiatry* **15**, 237-249 (2010).
- 906 57. Svenningsson, P., *et al.* Involvement of AMPA receptor phosphorylation in  
907 antidepressant actions with special reference to tianeptine. *Eur J Neurosci*  
908 **26**, 3509-3517 (2007).
- 909 58. Szegedi, V., *et al.* Tianeptine potentiates AMPA receptors by activating  
910 CaMKII and PKA via the p38, p42/44 MAPK and JNK pathways.  
911 *Neurochem Int* **59**, 1109-1122 (2011).
- 912 59. Monteggia, L.M., *et al.* Essential role of brain-derived neurotrophic factor  
913 in adult hippocampal function. *Proc Natl Acad Sci U S A* **101**, 10827-10832  
914 (2004).
- 915 60. Saarelainen, T., *et al.* Activation of the TrkB neurotrophin receptor is  
916 induced by antidepressant drugs and is required for antidepressant-  
917 induced behavioral effects. *J Neurosci* **23**, 349-357 (2003).
- 918 61. Ben M'Barek, K., *et al.* Huntingtin mediates anxiety/depression-related  
919 behaviors and hippocampal neurogenesis. *J Neurosci* **33**, 8608-8620  
920 (2013).
- 921 62. Orvoen, S., Pla, P., Gardier, A.M., Saudou, F. & David, D.J. Huntington's  
922 disease knock-in male mice show specific anxiety-like behaviour and  
923 altered neuronal maturation. *Neurosci Lett* **507**, 127-132 (2012).
- 924 63. Wheeler, V.C., *et al.* Long glutamine tracts cause nuclear localization of a  
925 novel form of huntingtin in medium spiny striatal neurons in HdhQ92 and  
926 HdhQ111 knock-in mice. *Hum Mol Genet* **9**, 503-513 (2000).
- 927 64. Pineda, J.R., *et al.* Genetic and pharmacological inhibition of calcineurin  
928 corrects the BDNF transport defect in Huntington's disease. *Mol Brain* **2**,  
929 33 (2009).
- 930 65. Humbert, S., *et al.* The IGF-1/Akt pathway is neuroprotective in  
931 Huntington's disease and involves Huntingtin phosphorylation by Akt.  
932 *Dev Cell* **2**, 831-837 (2002).
- 933 66. Pardo, R., *et al.* Inhibition of calcineurin by FK506 protects against  
934 polyglutamine-huntingtin toxicity through an increase of huntingtin  
935 phosphorylation at S421. *J Neurosci* **26**, 1635-1645 (2006).
- 936 67. Yasuda, R. Studying signal transduction in single dendritic spines. *Cold*  
937 *Spring Harb Perspect Biol* **4**(2012).
- 938 68. Mendez-David, I., *et al.* Rapid anxiolytic effects of a 5-HT(4) receptor  
939 agonist are mediated by a neurogenesis-independent mechanism.  
940 *Neuropsychopharmacology* **39**, 1366-1378 (2014).

942

943

944

945

946

947

948

949

950

951

952

953

954

955

956

957

958

959

960

961

962

963

964

965

966

967



968 **FIGURE LEGENDS**

969 **Figure 1** Deregulated GluA2-AMPA surface diffusion in different complementary HD  
970 cellular models **(a)** Experimental scheme showing that for endogenous GluA2-AMPA  
971 surface tracking, hippocampal neurons were incubated with mouse monoclonal antibody  
972 against N-terminal extracellular domain of GluA2 subunit followed by QD anti-mouse IgG.  
973 **(b)** Typical GluA2-QD trajectories (red) in hippocampal neurons expressing vector, exon1-  
974 wHTT and exon1-polyQ-HTT, respectively. Lower panels represent enlarged GluA2-QD  
975 trajectories. Scale bars, 10 $\mu$ m. **(c, d, e)** Top panels, GluA2-AMPA diffusion coefficients  
976 (median  $\pm$  25-75% interquartile range (IQR)) in rat hippocampal neurons expressing vector,  
977 exon1-wHTT, and exon1-polyQ-HTT; n = 844, 382 and 695 trajectories, respectively **(c)**, in  
978 hippocampal neurons from R6/1 mice and WT littermate controls; n =1885 and 1994  
979 trajectories, respectively **(d)**, and in hippocampal neurons from *Hdh*<sup>Q111/Q111</sup> mice and WT  
980 littermate controls; n =1571 and 886 trajectories, respectively **(e)**. Bottom panels, cumulative  
981 probability of GluA2 diffusion coefficient of respective top panel. The first point of the  
982 probability corresponding to the fraction of immobile receptors with diffusion coefficients  $\leq$   
983 0.01  $\mu$ m<sup>2</sup>/s was showed by arrows. Note that the cumulative curve shifts toward right  
984 indicating an increased GluA2 surface diffusion. Significance was determined by Kruskal-  
985 Wallis test followed by Dunn's Multiple Comparison Test **(c)**, or Mann-Whitney test **(d, e)**.  
986 \*\*\**P* < 0.001.

987

988 **Figure 2** GluA2-AMPA in polyQ-HTT-expressing neurons failed to stabilize on the  
989 neuronal surface after chemical LTP (cLTP) stimulation. **(a, b)** Top-left panels,  
990 epifluorescence image of a dendritic segment co-expressing Homer1c-EGFP (synaptic  
991 marker) and FL-wHTT **(a)** or FL-polyQ-HTT **(b)**; middle- and bottom-left panels,  
992 corresponding super-resolution image of endogenous GluA2-AMPA trajectories  
993 accumulated from 2000 images before (middle-left panels) and after cLTP stimulation  
994 (bottom-left panels) for the outlined region in the epifluorescence image. Scale bars, 10 $\mu$ m.  
995 Top-right panels, enlarged typical GluA2-AMPA trajectories before (black) and after cLTP

996 induction (red) in FL-wHTT- **(a)** and FL-polyQ-HTT-expressing neurons **(b)**. Scale bars,  
997 10 $\mu$ m. Bottom-right panels, the ratio of mobile to immobile fraction of the diffusion  
998 coefficient (D) before and after cLTP induction in FL-wHTT- **(a)** and FL-polyQ-HTT-  
999 expressing neurons **(b)**. Immobile fraction was identified as the proportion of receptors with  
1000  $D \leq 0.01 \mu\text{m}^2/\text{s}$  while mobile fraction with  $D > 0.01 \mu\text{m}^2/\text{s}$ . Paired t-test was used. \* $P < 0.05$ ;  
1001 *ns*, not significant.

1002

1003 **Figure 3** Impaired BDNF-TrkB-CaMKII signaling through the interaction between stargazin  
1004 and PSD95 contributes to the deregulation of AMPAR surface diffusion in HD models **(a)**  
1005 Schematic diagram showing that BDNF can be modulated at synthesis, transport and  
1006 secretion level. **(b)** Hippocampal BDNF protein level determined by ELISA in R6/1 and  
1007 *Hdh*<sup>Q111/Q111</sup> mice; values are mean  $\pm$  s.e.m (% of WT); n = 21 and 14 mice for WT and R6/1;  
1008 n = 6 and 9 mice for WT and *Hdh*<sup>Q111/Q111</sup>, respectively. **(c)** Representative kymographs of  
1009 intracellular transport of BDNF-containing vesicles (white trajectories) in a neurite (50  $\mu$ m  
1010 from soma) over 75 seconds (s) in wHTT- and polyQ-HTT-expressing rat hippocampal  
1011 neurons. The velocity of BDNF transport was reflected by the slope of trajectories (moving  
1012 distance against time). **(d, e, f)** Anterograde and retrograde BDNF transport velocity in all  
1013 neurites of wHTT- and polyQ-HTT-expressing rat hippocampal neurons **(d)**, and  
1014 hippocampal neurons from R6/1 mouse line **(e)**, and in the axon of hippocampal neurons from  
1015 *Hdh*<sup>Q111/Q111</sup> mouse line **(f)**; values are mean  $\pm$  s.e.m; n = 5569, 5656, 5227 and 5706  
1016 trajectories for anterograde and retrograde wHTT and polyQ-HTT, respectively; n = 1424,  
1017 1710, 1376, and 1487 trajectories for anterograde and retrograde WT and R6/1, respectively;  
1018 n = 236, 261, 194 and 256 trajectories for anterograde and retrograde WT and *Hdh*<sup>Q111/Q111</sup>,  
1019 respectively. **(g, h, i)** GluA2-AMPA diffusion coefficients in rat hippocampal neurons co-  
1020 expressing FL-wHTT/polyQ-HTT and GFP, or FL-polyQ-HTT and CamKII-GFP; n = 656,  
1021 685, and 349 trajectories, respectively **(g)**, in neurons co-expressing FL-polyQ-HTT and GFP  
1022 and treated with Vehicle, BDNF, TrkB-Fc plus BDNF, or kn93 plus BDNF; n = 1649, 1742,  
1023 480, and 1380 trajectories, respectively **(h)**, and in vehicle- or BDNF-treated neurons co-

1024 expressing FL-polyQ-HTT and GFP or GFP fused wild-type stargazin (Wt-stg-GFP), or  $\Delta$ C  
1025 stg, in which the binding domain to PSD95 was deleted; n = 495, 568, 376, 300, 573 and 498  
1026 trajectories, respectively (**i**). Diffusion coefficients were shown as median  $\pm$  25-75% IQR;  
1027 significance was determined by unpaired two-tailed Student's *t*-test (**b**, **d**, **e**, **f**), and Kruskal-  
1028 Wallis test followed by Dunn's Multiple Comparison Test (**g**, **h**, **i**); \**P* < 0.05, \*\**P* < 0.01,  
1029 \*\*\**P* < 0.001.

1030

1031 **Figure 4** Antidepressant tianeptine rescued the reduced BDNF protein level and intracellular  
1032 transport in different complementary HD models. (**a**, **b**, **c**) R6/1 mice were treated with saline  
1033 (vehicle) or tianeptine (25 mg/kg, i.p. daily) for 4 days. Hippocampal BDNF protein level was  
1034 assessed using ELISA Kit (**a**); values are mean  $\pm$  s.e.m (% of vehicle); n = 14 and 13 mice for  
1035 vehicle- and tianeptine-treated R6/1 group, respectively. Mature BDNF (mBDNF) and tubulin  
1036 (for normalization) were analyzed by immunoblot (**b**); quantified densitometry of 14 KDa  
1037 mBDNF, was expressed as percentage relative to tubulin (**c**); n = 9 and 7 mice for vehicle-  
1038 and tianeptine-treated R6/1 group, respectively. (**d**) *Hdh*<sup>Q111/Q111</sup> mice received one injection  
1039 of saline or tianeptine (10mg/kg, i.p.). Hippocampal BDNF protein level was evaluated using  
1040 ELISA kit; values are mean  $\pm$  s.e.m (% of vehicle); n = 9 and 8 mice for vehicle- and  
1041 tianeptine-treated *Hdh*<sup>Q111/Q111</sup> group, respectively. (**e**) Representative kymographs of  
1042 intracellular transport of BDNF-containing vesicles (white trajectories) in a neurite (35  $\mu$ m  
1043 from soma) over 75 seconds (s) in vehicle- or tianeptine-treated rat hippocampal neurons  
1044 expressing wHTT or polyQ-HTT. (**f**, **g**, **h**) Anterograde and retrograde BDNF transport  
1045 velocity in all neurites of vehicle- or tianeptine-treated wHTT- and polyQ-HTT-expressing rat  
1046 hippocampal neurons (**f**), of hippocampal neurons from vehicle- or tianeptine-treated R6/1  
1047 mice and WT littermates (**g**), and in the axon of hippocampal neurons from vehicle- or  
1048 tianeptine-treated *Hdh*<sup>Q111/Q111</sup> and WT mice (**h**); values are mean  $\pm$  s.e.m; n = 5569, 5656,  
1049 3339, 5737, 5227, 5706, 3190, and 5663 trajectories for anterograde and retrograde BDNF  
1050 velocity in wHTT-vehicle, polyQ-HTT-vehicle, and polyQ-HTT-tianeptine (10 and 50  $\mu$ M)  
1051 neurons, respectively; n = 1424, 1710, 1512, 1376, 1487, and 1238 trajectories for

1052 anterograde and retrograde velocity in WT-vehicle, R6/1-vehicle, and R6/1-tianeptine (50  
1053  $\mu\text{M}$ ) neurons, respectively;  $n = 236, 261, 432, 194, 256,$  and 357 trajectories for anterograde  
1054 and retrograde velocity in WT-vehicle, *Hdh*<sup>Q111/Q111</sup>-vehicle, and *Hdh*<sup>Q111/Q111</sup>-tianeptine (10  
1055  $\mu\text{M}$ ) neurons, respectively. Significance was determined by unpaired two-tailed Student's *t*-  
1056 test (**a, c, d**), and one-way ANOVA followed Bonferroni's Multiple Comparison Test (**f, g, h**);  
1057 \* $P < 0.05$ , \*\* $P < 0.01$ , \*\*\* $P < 0.001$ .

1058

1059 **Figure 5** Tianeptine's effect on BDNF intracellular transport and AMPAR surface diffusion  
1060 is likely mediated by BDNF-TrkB signaling pathway. **(a)** Representative kymographs of  
1061 intracellular transport of BDNF-containing vesicles (white trajectories) in a neurite (50  $\mu\text{m}$   
1062 from soma) over 75 seconds (s) in polyQ-HTT-expressing rat hippocampal neurons treated  
1063 with vehicle, tianeptine or cyclotraxin-B (CB) plus tianeptine. **(b, c)** Anterograde and  
1064 retrograde BDNF transport velocity in all neurites of polyQ-HTT-expressing rat hippocampal  
1065 neurons treated with vehicle, tianeptine or CB plus tianeptine **(b)**, or treated with vehicle,  
1066 BDNF, tianeptine, or BDNF plus tianeptine **(c)**; values are mean  $\pm$  s.e.m;  $n = 4322, 4017,$   
1067 4199, 4354, 3887, and 3954 trajectories for anterograde and retrograde velocity in polyQ-  
1068 HTT-expressing neurons treated with vehicle, tianeptine, and CB plus tianeptine, respectively  
1069 **(b)**;  $n = 3505, 3382, 3339, 2099, 3346, 3174, 3190$  and 2022 trajectories for anterograde and  
1070 retrograde velocity in polyQ-HTT-expressing neurons treated with vehicle, BDNF, tianeptine,  
1071 and BDNF plus tianeptine, respectively **(c)**. **(d)** Typical GluA2-QD trajectories (red) in  
1072 polyQ-HTT-expressing rat hippocampal neurons, treated with vehicle, tianeptine, CB plus  
1073 tianeptine, or TrkB-Fc plus tianeptine. Scale bars, 10 $\mu\text{m}$ . **(e)** GluA2-AMPA diffusion  
1074 coefficients in FL-polyQ-HTT-expressing rat hippocampal neurons treated with vehicle,  
1075 tianeptine, CB plus tianeptine, or TrkB-Fc plus tianeptine; data are shown as median  $\pm$  25-  
1076 75% IQR;  $n = 601, 535, 708,$  and 556 trajectories for 4 groups, respectively. Significance was  
1077 assessed by one-way ANOVA followed Bonferroni's Multiple Comparison Test (**b, c**) or  
1078 Kruskal-Wallis test followed by Dunn's Multiple Comparison Test **(e)**; \* $P < 0.05$ , \*\* $P <$   
1079 0.01, \*\*\* $P < 0.001$ ; *ns*, not significant.

1080

1081 **Figure 6** Tianeptine rescued impaired hippocampal CA1 LTP and hippocampus-dependent  
1082 memory as well as anxiety/depression like behavior in different complementary HD mouse  
1083 models. **(a, b)** Field EPSPs (fEPSPs) were recorded in CA1 region-containing acute slices of  
1084 vehicle- or tianeptine-treated R6/1 **(a)** and *Hdh<sup>Q111Q111</sup>* mice **(b)** following theta-burst  
1085 stimulation of the Schaffer collaterals. Recording of fEPSPs was carried out blind with  
1086 respect to genotype or treatment. Bar graph showing the percentage of potentiation observed  
1087 during last 5-10 min of each recording; data are mean  $\pm$  s.e.m; n = 16, 24, and 26 slices for  
1088 vehicle-treated WT and R6/1 mice and tianeptine-treated R6/1 mice; n = 6, 11, 18, 16 slices  
1089 for untreated WT, *Hdh<sup>Q111Q111</sup>* mice and glucose- and tianeptine- treated *Hdh<sup>Q111Q111</sup>* mice. **(c, d)**  
1090 Hippocampus-dependent memory was examined using Y-maze **(c)** and contextual fear  
1091 conditioning paradigm **(d)** in vehicle- or tianeptine-treated R6/1 and WT littermate mice. **(c)**  
1092 Left, schematic diagram for Y-maze; right, percentage of time spent by mice in novel arms to  
1093 that in total arms during 2-minute testing time. **(d)** Left, schematic diagram for contextual fear  
1094 conditioning; right, freezing time during 3- minute testing time; data are mean  $\pm$  s.e.m; n =  
1095 25, 28, 33, and 32 mice **(c)** and n = 10, 10, 10, and 12 mice **(d)** for vehicle- and tianeptine-  
1096 treated WT and R6/1 mice. **(e, f)** Anxiety/ depression-like behaviors were evaluated with  
1097 elevated plus maze (EPM)**(e)** and novelty-suppressed feeding (NSF) paradigm **(f)** in HD  
1098 CAG140 knock-in mice and WT littermates. **(e)** Left, schematic diagram for EPM; right, time  
1099 spent in opened arms in EPM, which is an anxiety index. **(f)** Values plotted are cumulative  
1100 survival of animals that did not eat over 15 minutes (left) or mean of latency to feed in  
1101 seconds  $\pm$  s.e.m (right). The latency to begin eating is an index of anxiety/depression-like  
1102 behavior; n = 12, 9, 14, and 13 mice for vehicle- and tianeptine-treated WT and CAG140  
1103 mice **(e, f)**. Significance was assessed by one-way ANOVA followed by Bonferroni's  
1104 Multiple Comparison Test **(a, b)**, and two-way ANOVA followed by Bonferroni posttests **(c,**  
1105 **d, e, f)**. \* $P < 0.05$ , \*\* $P < 0.01$ , \*\*\* $P < 0.001$ .

1106

1107

1108  
1109  
1110

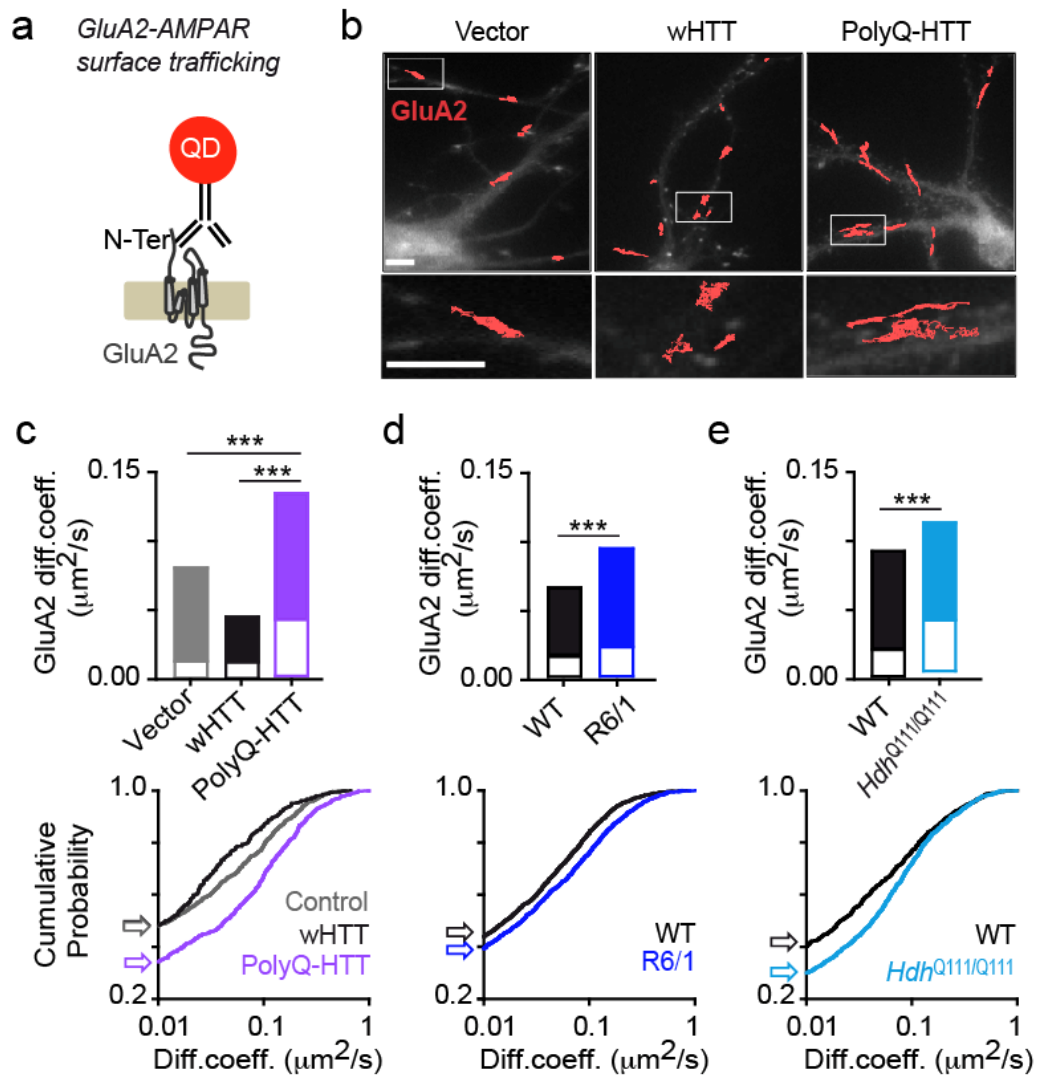


Figure 1

1111  
1112  
1113  
1114  
1115  
1116  
1117  
1118  
1119  
1120  
1121  
1122  
1123  
1124  
1125

1126

1127

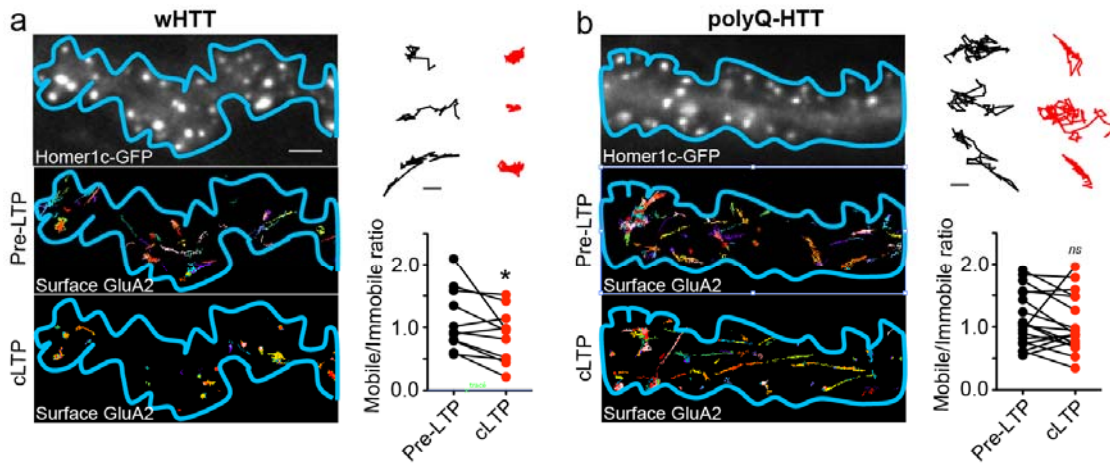


Figure 2

1128

1129

1130

1131

1132

1133

1134

1135

1136

1137

1138

1139

1140

1141

1142

1143

1144

1145

1146

1147

1148

1149

1150

1151

1152

1153

1154

1155

1156

1157

1158

1159

1160



1161  
1162  
1163

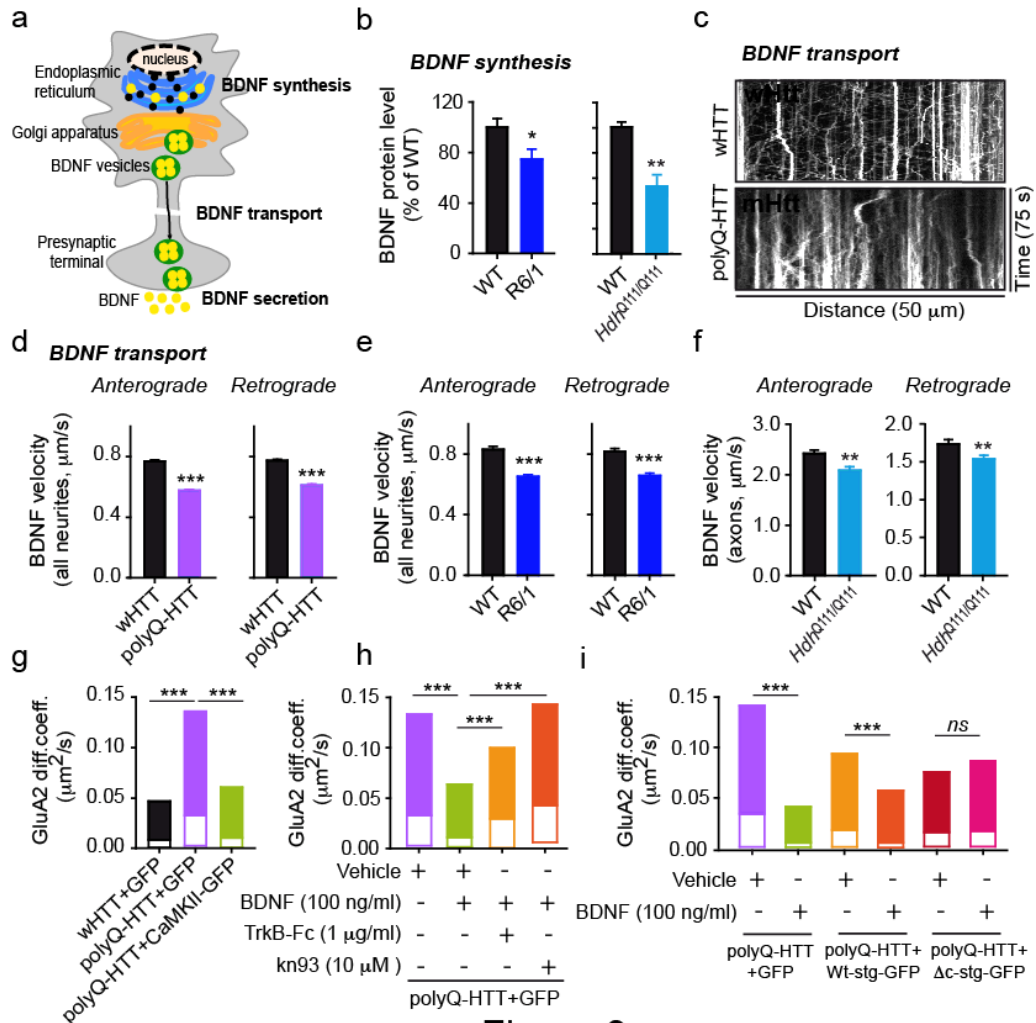


Figure 3

1164  
1165  
1166  
1167  
1168  
1169  
1170  
1171  
1172  
1173  
1174  
1175  
1176  
1177  
1178  
1179  
1180



1181

1182

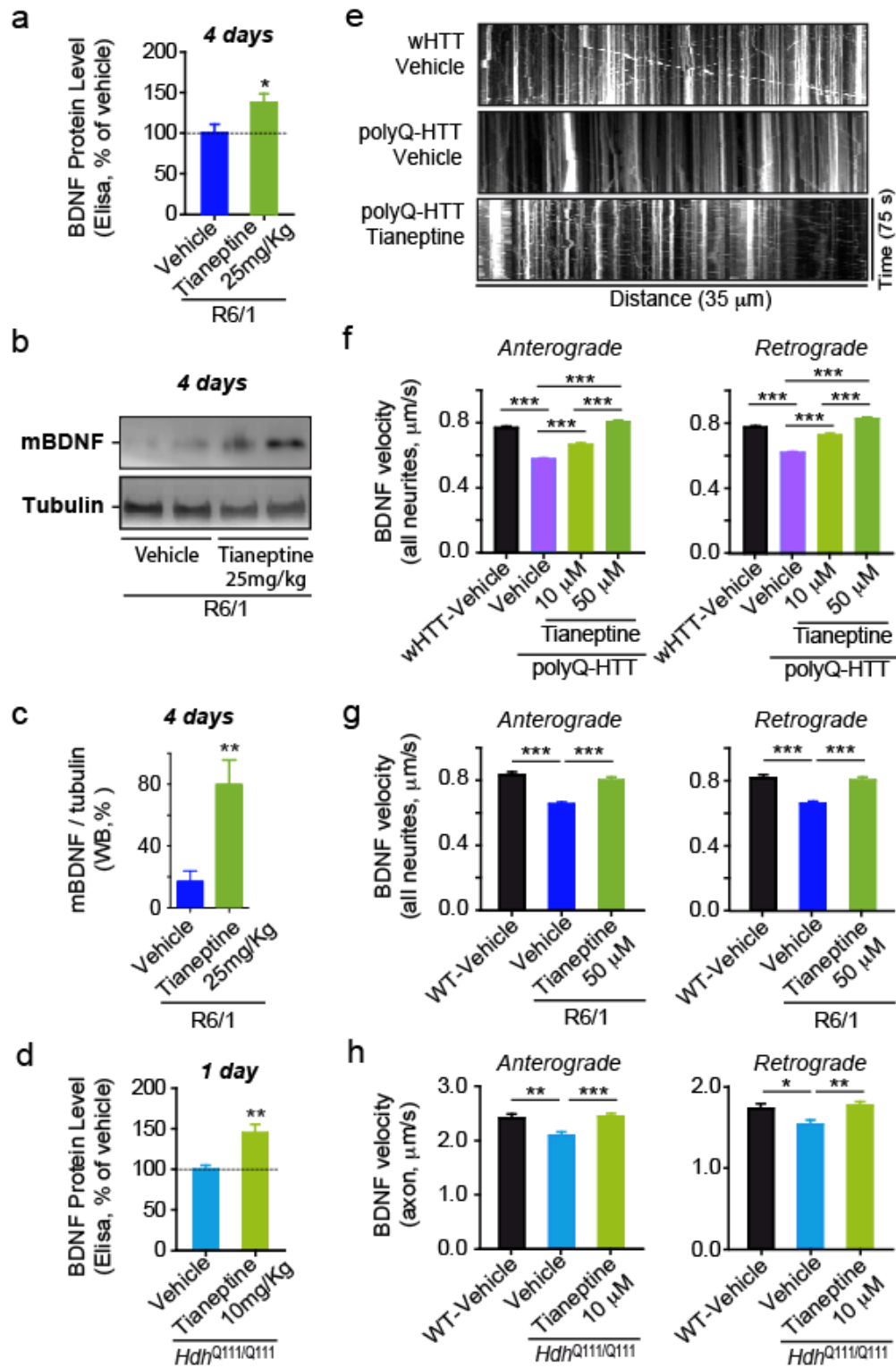


Figure 4

1183

1184

1185

1186  
1187

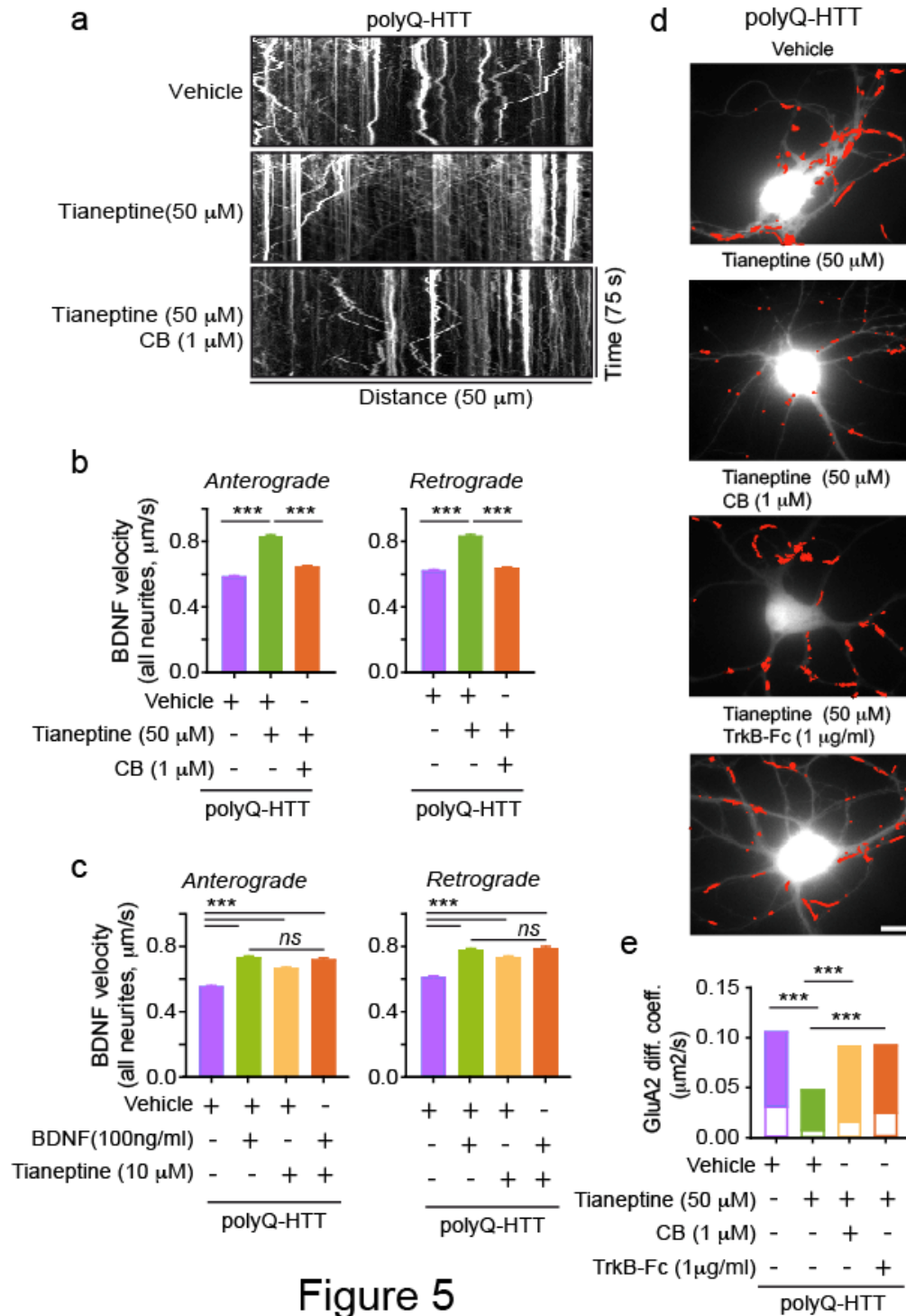


Figure 5

1188  
1189  
1190  
1191  
1192  
1193  
1194

1195  
1196

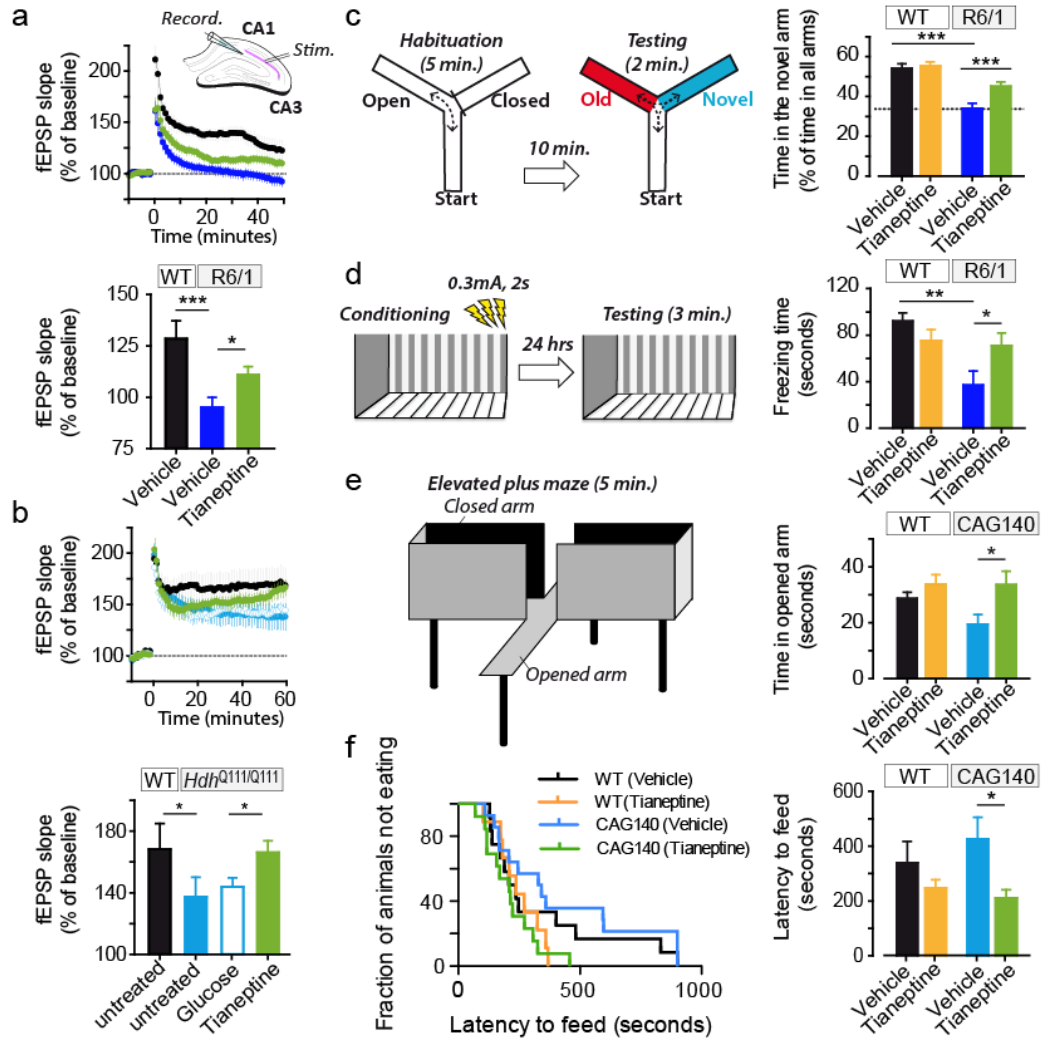


Figure 6

1197  
1198  
1199  
1200  
1201  
1202

1 **Pharmacological modulation of AMPA receptor surface diffusion restores hippocampal**  
2 **synaptic plasticity and memory in Huntington's disease**

3

4 **Supplementary material**

5

6 Hongyu Zhang<sup>1, 2</sup>, Chunlei Zhang<sup>1, 2</sup>, Jean Vincent<sup>1, 2</sup>, Diana Zala<sup>3, 4</sup>, Caroline Benstaali<sup>5, 6</sup>,

7 Matthieu Sainlos<sup>1, 2</sup>, Dolores Grillo-Bosch<sup>1, 2</sup>, Yoon Cho<sup>7</sup>, Denis J. David<sup>8</sup>, Frederic Saudou<sup>5, 6</sup>,

8 <sup>9</sup>, Yann Humeau<sup>1, 2</sup>, Daniel Choquet<sup>1, 2, 10-12</sup>

9

10

11

12 **Supplemental Figure 1** Deregulated GluA1-AMPA surface diffusion in rat hippocampal  
13 neurons expressing FL-polyQ-HTT **(a)** Experimental scheme showing that for endogenous  
14 GluA1-AMPA surface tracking, hippocampal neurons were incubated with rabbit  
15 polyclonal antibody against N-terminal extracellular domain of GluA1 subunit followed by  
16 QD anti-rabbit IgG. **(b)** Left, GluA1-AMPA diffusion coefficients in rat hippocampal  
17 neurons expressing FL-wHTT or FL-polyQ-HTT; data are shown as median  $\pm$  25-75% IQR;  
18  $n = 206$  and  $310$  trajectories, respectively. right, cumulative probability of GluA1 diffusion  
19 coefficient. The first point of the probability corresponding to the fraction of immobile  
20 receptors with diffusion coefficients  $\leq 0.01 \mu\text{m}^2/\text{s}$  was showed by arrows. The cumulative  
21 curve of FL-polyQ-HTT expressing neurons shifts toward right implying an increased  
22 GluA1-AMPA surface diffusion. Significance was determined by Mann-Whitney test. **\*\*\*** $P$   
23  $< 0.001$ .

24

25 **Supplemental Figure 2** Decreased CaMKII activity in HD cellular model **(a)** Schematic  
26 diagram showing fluorescence resonance energy transfer (FRET)-based CaMKII $\alpha$ , named  
27 REACH-CaMKII $\alpha$ . The activation of REACH-CaMKII changes the conformation to the open  
28 state in which its kinase domain is exposed, thereby decreasing FRET and increasing the  
29 fluorescence lifetime of mEGFP. **(b)** Representative lifetime image of rat hippocampal  
30 neurons expressing PDS95-GFP, REACH-CaMKII $\alpha$  plus FL-wHTT, and REACH-CaMKII $\alpha$   
31 plus FL-polyQ-HTT. Blue color indicates strong FRET and short lifetime, while red color  
32 represents weak FRET and long lifetime. **(c, d)** Quantification of lifetime in randomly-  
33 selected regions in dendritic puncta **(c)** or in dendritic shaft **(d)** in rat hippocampal neurons  
34 expressing PDS95-GFP, REACH-CaMKII $\alpha$  plus FL-wHTT, or REACH-CaMKII $\alpha$  plus FL-  
35 polyQ-HTT. PDS95-GFP-expressing neurons showed long lifetime ( $\geq 2.4$  ns) in both  
36 dendritic puncta and shaft indicating no FRET. Lower lifetime indicates stronger FRET and  
37 reduced CaMKII $\alpha$  activity; data are mean  $\pm$  s.e.m;  $n = 178$ ,  $231$ , and  $238$  regions for dendritic  
38 puncta, and  $n = 93$ ,  $115$  and  $188$  regions for dendritic shaft in neurons expressing PDS95-  
39 GFP, REACH-CaMKII $\alpha$  plus FL-wHTT, and REACH-CaMKII $\alpha$  plus FL-polyQ-HTT,

40 respectively. Significance was assessed by One-way ANOVA followed by Bonferroni's  
41 Multiple Comparison Test; \*\*\*  $P < 0.001$ .

42

43 **Supplemental Figure 3** Tianeptine facilitated BDNF intracellular transport in wHTT-  
44 expressing rat hippocampal neurons and neurons from WT mice. **(a, b)** Anterograde and  
45 retrograde BDNF transport velocity in all neurites of vehicle- or tianeptine-treated wHTT-  
46 expressing rat hippocampal neurons **(a)**, and in the axon of hippocampal neurons from WT  
47 mice for *Hdh*<sup>Q111/Q111</sup> mouse line **(b)**; values are mean  $\pm$  s.e.m; n = 5569, 2522, 5227 and 2542  
48 trajectories for anterograde and retrograde BDNF velocity in vehicle and tianeptine-treated  
49 wHTT-expressing neurons, respectively; n = 236, 157, 194 and 110 trajectories for  
50 anterograde and retrograde BDNF velocity in vehicle and tianeptine-treated neurons from WT  
51 mice for *Hdh*<sup>Q111/Q111</sup> mouse line. Significance was determined by unpaired two-tailed  
52 Student's *t*-test; \* $P < 0.05$ , \*\*\* $P < 0.001$ .

53

54 **Supplemental Figure 4** Tianeptine did not affect moving velocity of R6/1 mice in Open  
55 Field test, not change ambulatory distance nor food assumption of HTT CAG140 mice in  
56 elevated plus maze (EPM) and novelty-suppressed feeding (NSF), respectively. **(a)** Moving  
57 velocity in open field was significantly different between genotype but not between treatment;  
58 values are mean  $\pm$  s.e.m; n = 25, 28, 33 and 32 mice for vehicle- and tianeptine-treated WT  
59 and R6/1 mice, respectively. **(b)** In EPM, there is no significant change in the locomotor  
60 activity between genotype nor treatment, which is revealed by ambulatory distance. **(c)** In  
61 NSF, food consumption was not significantly different between genotype nor treatment;  
62 values are mean  $\pm$  s.e.m; n = 12, 9, 14, and 13 mice for vehicle- and tianeptine-treated WT  
63 and HTT CAG140 mice, respectively. Significance was assessed by two-way ANOVA  
64 followed by Bonferroni posttests **(a, b, c)**. \*\*\* $P < 0.001$ ; *ns*, not significant.

65

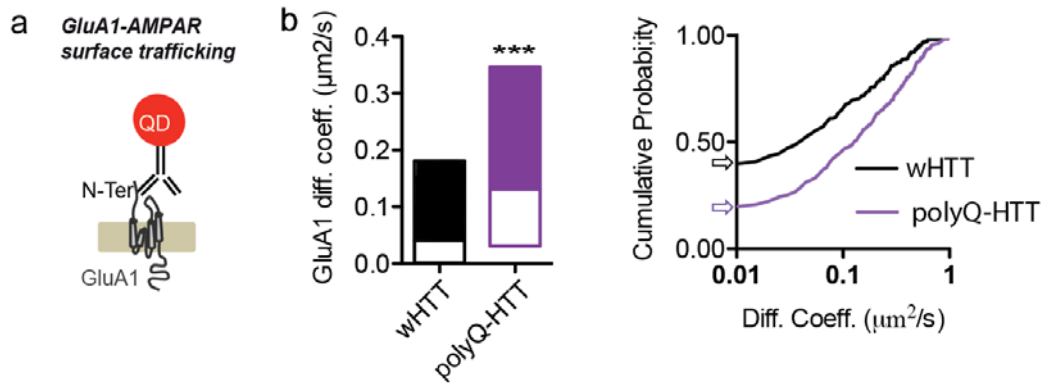
66

67

68

69  
70  
71  
72  
73  
74  
75  
76  
77  
78  
79  
80  
81

82  
83

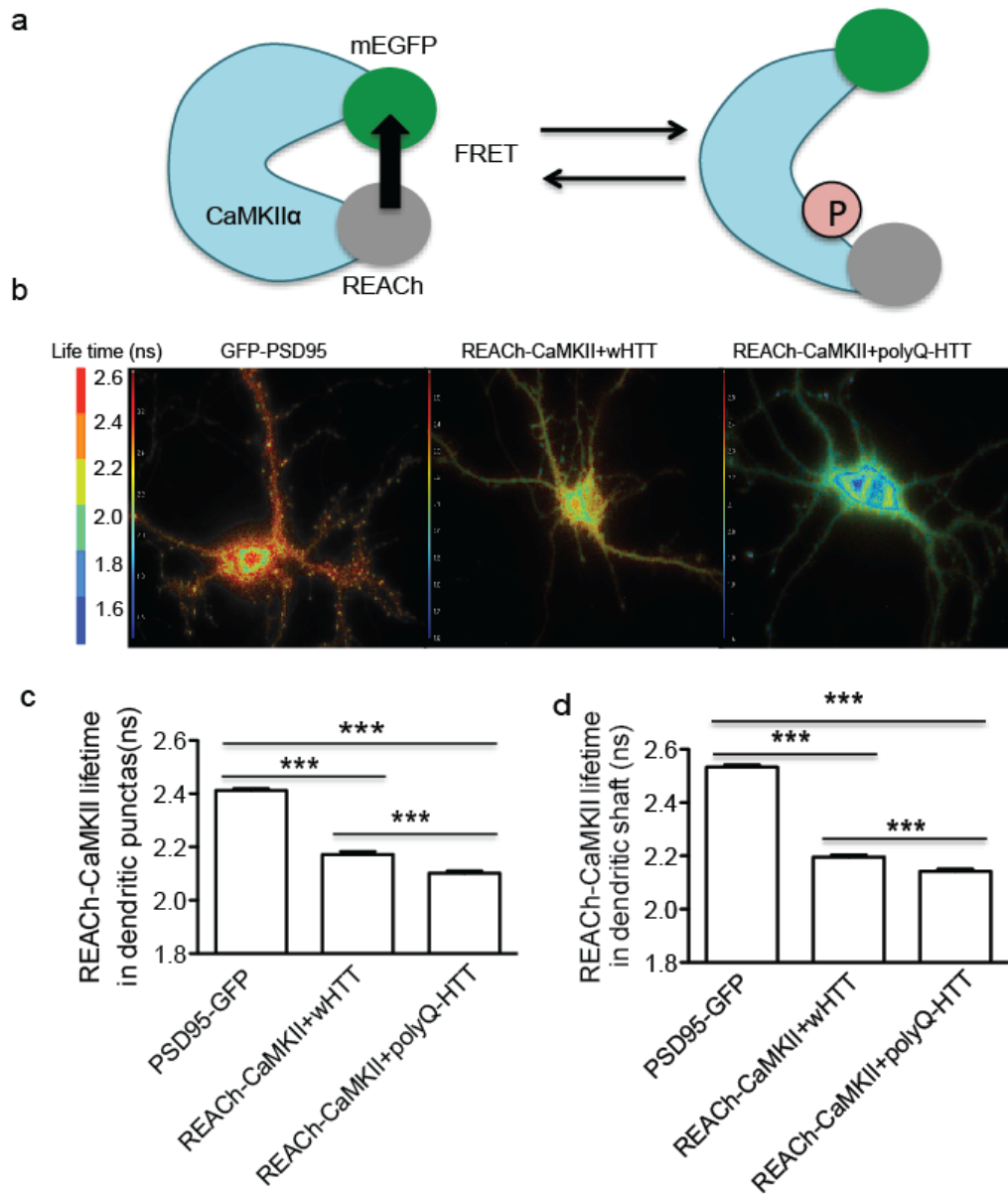


Supplemental Figure 1

84  
85  
86  
87  
88  
89  
90  
91  
92  
93  
94  
95  
96  
97  
98  
99  
100  
101  
102  
103  
104  
105  
106  
107  
108  
109  
110  
111  
112  
113  
114  
115  
116  
117  
118  
119

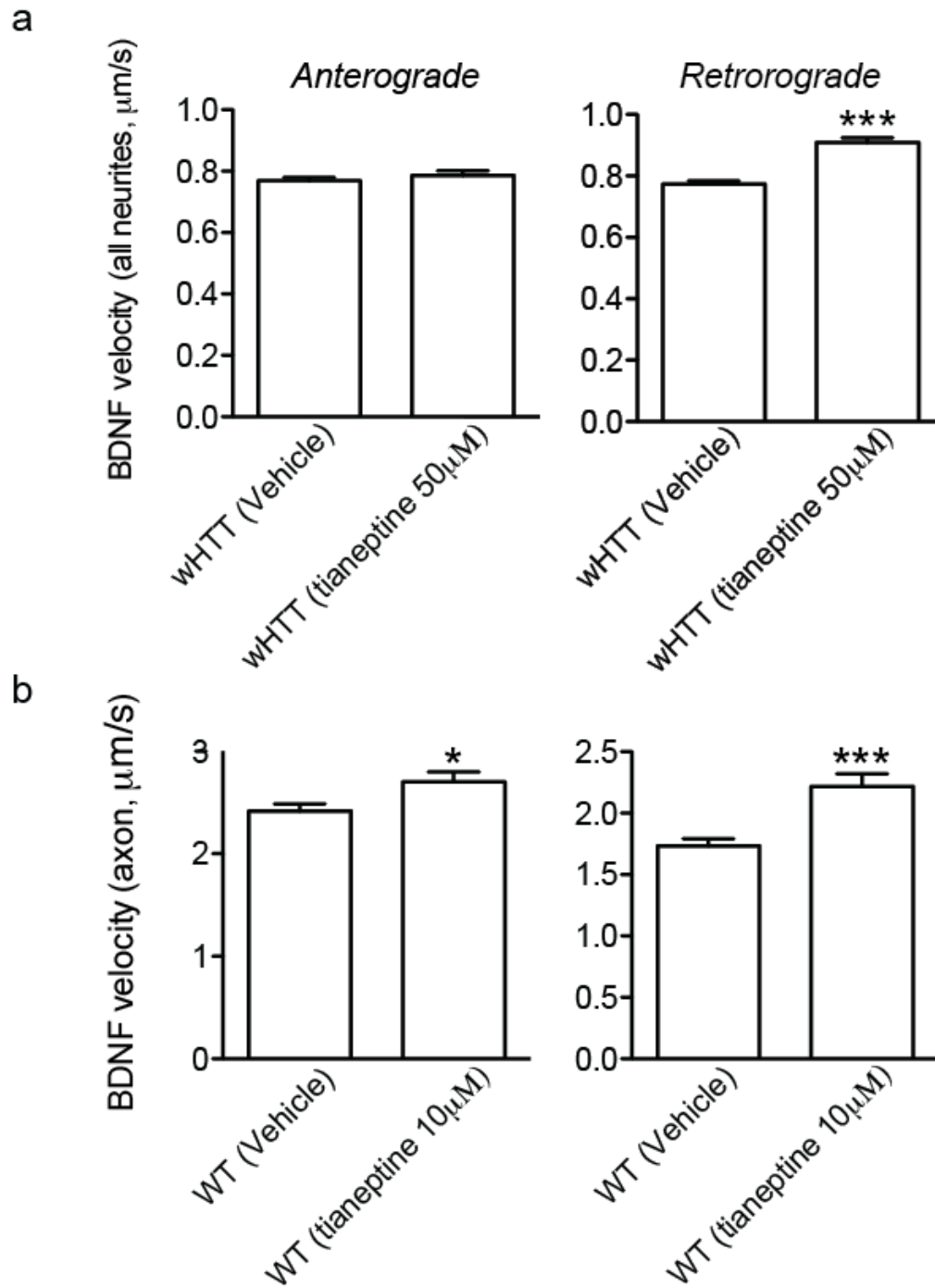


120  
121



122  
123  
124  
125  
126  
127  
128  
129  
130  
131  
132  
133

134  
135  
136  
137

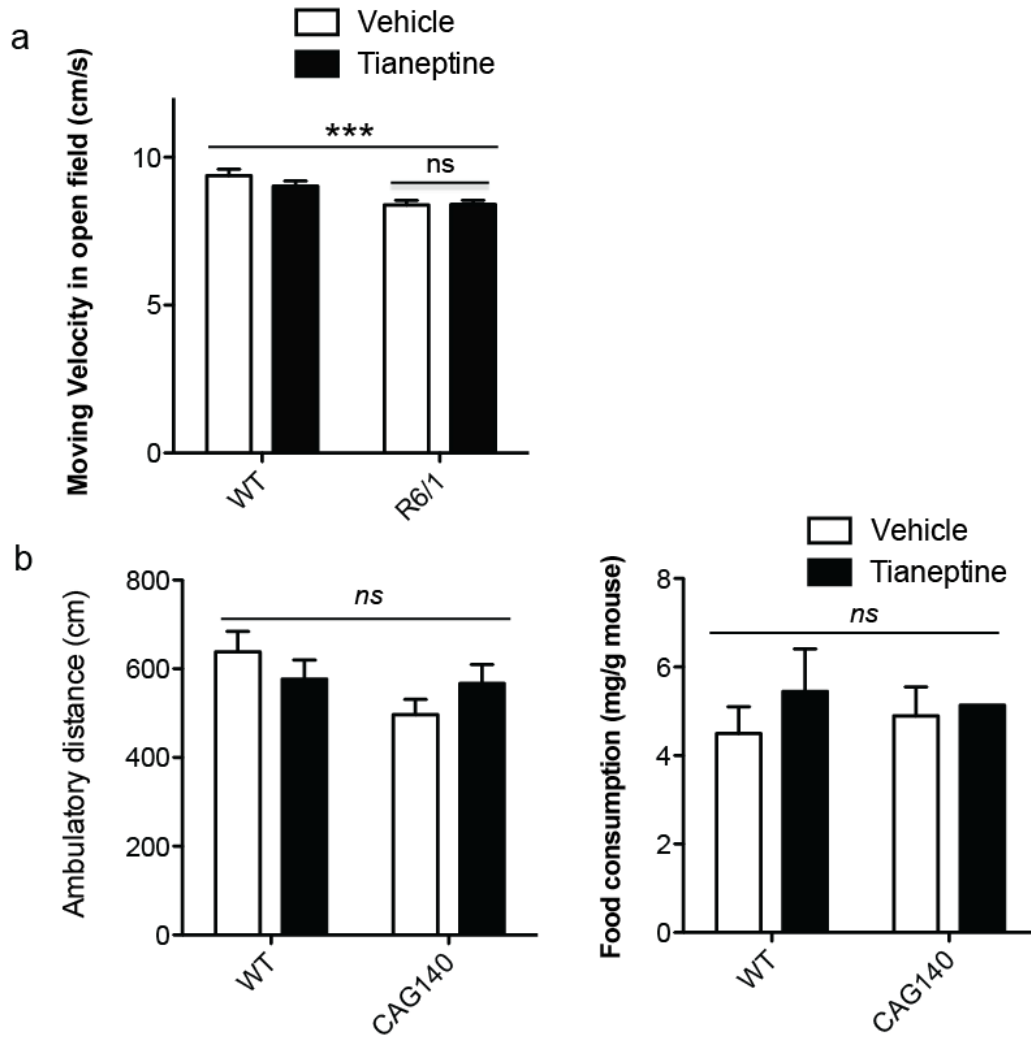


Supplemental Figure 3

138  
139  
140  
141

142

143



Supplemental Figure 4

144